Expansion and contraction of the umbrella cell apical junctional ring in response to bladder filling and voiding

Amity F. Eaton[a,b], Dennis R. Clayton[a], Wily G. Ruiz[a], Shawn E. Griffiths[a], Maria Eulalia Rubio[c], and Gerard Apodaca[a,b,*]

[a]Department of Medicine, George M. O'Brien Pittsburgh Center for Kidney Research, [b]Department of Cell Biology, and [c]Department of Neurobiology, University of Pittsburgh School of Medicine, Pittsburgh, PA 15261

ABSTRACT **The epithelial junctional complex, composed of tight junctions, adherens junctions, desmosomes, and an associated actomyosin cytoskeleton, forms the apical junctional ring (AJR), which must maintain its continuity in the face of external mechanical forces that accompany normal physiological functions. The AJR of umbrella cells, which line the luminal surface of the bladder, expands during bladder filling and contracts upon voiding; however, the mechanisms that drive these events are unknown. Using native umbrella cells as a model, we observed that the umbrella cell's AJR assumed a nonsarcomeric organization in which filamentous actin and ACTN4 formed unbroken continuous rings, while nonmuscle myosin II (NMMII) formed linear tracts along the actin ring. Expansion of the umbrella cell AJR required formin-dependent actin assembly, but was independent of NMMII ATPase function. AJR expansion also required membrane traffic, RAB13-dependent exocytosis, specifically, but not trafficking events regulated by RAB8A or RAB11A. In contrast, the voiding-induced contraction of the AJR depended on NMMII and actin dynamics, RHOA, and dynamin-dependent endocytosis. Taken together, our studies indicate that a mechanism by which the umbrella cells retain continuity during cyclical changes in volume is the expansion and contraction of their AJR, processes regulated by the actomyosin cytoskeleton and membrane trafficking events.**

Monitoring Editor
Keith E. Mostov
University of California, San Francisco

Received: Feb 21, 2019
Revised: May 31, 2019
Accepted: May 31, 2019

INTRODUCTION

Umbrella cells form the outermost layer of the stratified bladder epithelium, or urothelium, and maintain one of the least permeable barriers in the body despite continuous cycles of bladder filling and voiding. This is made possible by several specializations. First, the umbrella cell transitions during filling from an inverted parasol shape to one that is flat and squamous, a change that is reversed upon voiding (Khandelwal *et al.*, 2009). Second, bladder filling stimulates a large subapical pool of vesicles to undergo RAB8A-, RAB11A-, and RAB27B-dependent exocytosis, dramatically increasing apical surface area (Apodaca, 2001b; Truschel *et al.*, 2002; Chen *et al.*, 2003; Khandelwal *et al.*, 2008b, 2013; Yu *et al.*, 2009; Wankel *et al.*, 2016; Gallo *et al.*, 2018). During voiding, the excess apical membrane is rapidly internalized by an integrin-triggered, DNM2 (dynamin-2)-dependent, RHOA-dependent, clathrin-independent endocytic pathway (Apodaca, 2001b; Truschel *et al.*, 2002; Khandelwal *et al.*, 2008, 2010, 2013). In addition to the barrier created by the umbrella cell apical plasma membrane, the umbrella cell apical junctional ring (AJR; composed of the tight junction, adherens junction, desmosomes, and associated actomyosin ring) is also critical for maintaining the uroepithelial barrier during the bladder cycle and must maintain proper structure and function in the face of changing wall tension during bladder filling and voiding. Understanding how the umbrella cell accomplishes this is the goal of this study.

The requirement that the AJR maintain its continuity in response to intrinsic and extrinsic mechanical forces (e.g., tension, compression, and shear stress) is not limited to umbrella cells, as all epithelial

This article was published online ahead of print in MBoC in Press (http://www.molbiolcell.org/cgi/doi/10.1091/mbc.E19-02-0115) on June 5, 2019.

*Address correspondence to: Gerard Apodaca (gla6@pitt.edu).

Abbreviations used: AJR, apical junctional ring; NMMII, nonmuscle myosin II.

cells are exposed to mechanical stimuli during development and during normal physiological functions such as lung inflation, fluid flow through the nephrons or vasculature, and bladder distension (Cavanaugh *et al.*, 2001; Thi *et al.*, 2004; Tzima *et al.*, 2005; Duan *et al.*, 2008; Carattino *et al.*, 2013; Rubsam *et al.*, 2018). Morphologically, this stretching alters the distribution of proteins associated with the tight junction (Cavanaugh *et al.*, 2001; Cohen *et al.*, 2010; Samak *et al.*, 2014; Song *et al.*, 2016) and affects junctional strand number and distribution (Pitelka *et al.*, 1973; Pitelka and Taggart, 1983; Metz *et al.*, 1977, 1978; Koga and Todo, 1978; Greven and Robenek, 1980; Akao *et al.*, 2000). Evidence is also emerging that tight junctions are intimately involved in mechanotransduction (Balda and Matter, 2008, 2016; Tornavaca *et al.*, 2015; Sluysmans *et al.*, 2017). For example, TJP1 (zonula-occludens 1; ZO-1) was recently shown to adopt an extended conformation in response to tension, which causes the TJP1-binding protein YBX3 (Dbpa/ZONAB) to relocate to the nucleus, where it functions as a transcription factor that triggers changes in gene expression, cell proliferation, and paracellular barrier function (Spadaro *et al.*, 2017). Much more is understood about the mechanosensitive properties of the adherens junction, which like the tight junction undergoes structural and compositional rearrangements in response to mechanical forces (Charras and Yap, 2018; Pinheiro and Bellaiche, 2018; Rubsam *et al.*, 2018). Here, forces generated by the contractile actomyosin ring, driven by nonmuscle myosin II (NMMII) contraction, stiffen junctional complexes formed by CDH1 (E-cadherin), as well as inducing a conformational change in CTTNA1 (α-catenin) allowing it to bind more strongly with CTTNB1 (β-catenin) and to form interactions with VCL (vinculin; Yao *et al.*, 2014). This promotes further AJR remodeling through recruitment of additional actin-binding proteins and altered actomyosin dynamics, eventually resulting in events such as cell polarization (Takeichi, 2018).

Mechanical forces, including those generated during cell–cell intercalation, wound closure, cell division, dorsal closure in *Drosophila*, cell extrusion, and epithelial invagination, are associated with constriction (i.e., reduction in cell perimeter) of the adherens junction, and presumably the entire AJR (Schwayer *et al.*, 2016). This constriction is driven by the RHOA-dependent activation of the formin DIAPH1 (mDia) pathway for actin polymerization (Homem and Peifer, 2008; Levayer *et al.*, 2011), and the RHOA- and ROCK-dependent activation of the NMMIIA complex (Kolesnikov and Beckendorf, 2007; Borges *et al.*, 2011; Itoh *et al.*, 2014; Sai *et al.*, 2014). Considering the close association between the cytoskeleton and membrane traffic (Valentijn *et al.*, 1999; Apodaca, 2001a, 2002; Croise *et al.*, 2014; Kjos *et al.*, 2018), it is not surprising that apical constriction in frogs and flies also depends on endocytosis, which is modulated by dynamin, Rab5, Rab35, and other regulators of the actomyosin cytoskeleton (Lee and Harland, 2010; Levayer *et al.*, 2011; Mateus *et al.*, 2011; Jewett *et al.*, 2017). However, whether endocytosis plays a similar role in vertebrate AJR constriction is not known.

In contrast to AJR constriction, there is a limited literature concerning the expansion of the AJR or the mechanisms that regulate these events. Following cell intercalation, a new cell–cell contact is added perpendicular to the site of junction constriction (Mateus *et al.*, 2011). This addition requires pulling forces generated by myosin flows in adjacent border cells (Yu and Fernandez-Gonzalez, 2016) and is likely to depend on the insertion of new membrane in the intercalated cells by exocytosis; however, this has not been shown conclusively (Shaye *et al.*, 2008). In the *Drosophila* pupal wing, junctional expansion requires the down-regulation of NMMII activity (Bardet *et al.*, 2013). Finally, in *Drosophila*, Rab11-dependent exocytosis promotes cell elongation, a process where the AJR increases in length along a single axis (Mateus *et al.*, 2011), and there is evidence that endothelial cells can increase the area of their adherens junction in response to stretch (Liu *et al.*, 2010).

We previously reported that the rat umbrella cell tight junction and associated actin ring expand by ~150% during filling, and return to their quiescent size after just five minutes of voiding (Carattino *et al.*, 2013). We hypothesized that the dynamic nature of the umbrella cell AJR likely serves as a mechanism to maintain umbrella cell barrier function in the face of large changes in bladder wall tension. In the current study, we asked whether the adherens junction was similarly affected during the bladder cycle, whether the organization and dynamics of the actomyosin cytoskeleton was affected by filling and voiding, and whether membrane traffic played a role in these events. Our studies indicate that both actomyosin dynamics and membrane trafficking events contribute to umbrella cell AJR expansion and contraction during the bladder cycle.

RESULTS

The actomyosin cytoskeleton associated with the AJR of bladder umbrella cells forms a nonsarcomeric network

When viewed en face, the outermost umbrella cell layer of the stratified urothelium is composed of large (up to 100 μm in diameter), typically binucleate, polyhedral cells that form an AJR at the apicolateral borders of adjacent cells (Figure 1). We previously reported that the average perimeter of the AJR per umbrella cell increased from ~160 μm in voided bladders to ~250 μm in filled bladders (Carattino *et al.*, 2013). Using the tight junction-associated protein CLDN8 (claudin-8) and the AJR-associated actin cytoskeleton (labeled with phalloidin) as markers, we confirmed that spontaneous bladder filling in anesthetized rats stimulated an expansion of the umbrella cell AJR, which was rapidly reversed within 5 min of voiding (compare filled bladders, marked with an "F," with those that were quiescent and never allowed to fill, marked with a "Q," or voided after filling, marked with a "V," in Figure 1A). The contracted AJR in voided bladders assumed a perimeter that was similar to that observed in quiescent bladders (compare "V" and "Q" in Figure 1A), indicating that the AJR contraction was complete within 5 min of bladder voiding. Using CDH1 as a marker, we also examined how the bladder cycle affected the adherens junction. Like the tight junction, the adherens junction ring expanded during bladder filling and rapidly contracted upon voiding (Figure 1B).

We next sought to understand the organization of the AJR-associated actin cytoskeleton in the umbrella cell, and whether its organization was impacted by filling and voiding. Like the tight junction and adherens junction, the perimeter of the subapical F-actin ring expanded with filling and contracted after voiding (Figure 1, A and B). Furthermore, and reflecting their close proximity within the AJR, the tight junction and adherens junction completely matched the contours of the F-actin ring during these transitions (Figure 1). At higher magnification, and within the limits of light microscopic resolution, the F-actin ring appeared as a single, continuous fine line between adjacent cells (Figure 1C), indicating that the plasma membranes of adjacent cells were very closely apposed in this region of the cell. During filling and voiding, there were no obvious effects on the continuity of the F-actin ring, which always appeared smooth, unbroken, and not periodic in nature. However, when three-dimensional (3D) reconstructions of the AJR at bicellular and tricellular junctions were examined, we noted that the position of the F-actin ring with respect to the tight junction changed. We observed that in filled bladders, the umbrella cell F-actin ring was readily resolved from the more apical tight junction, labeled with TJP1, or the subjacent CDH1-labeled adherens junction (Figure 1C). In contrast,

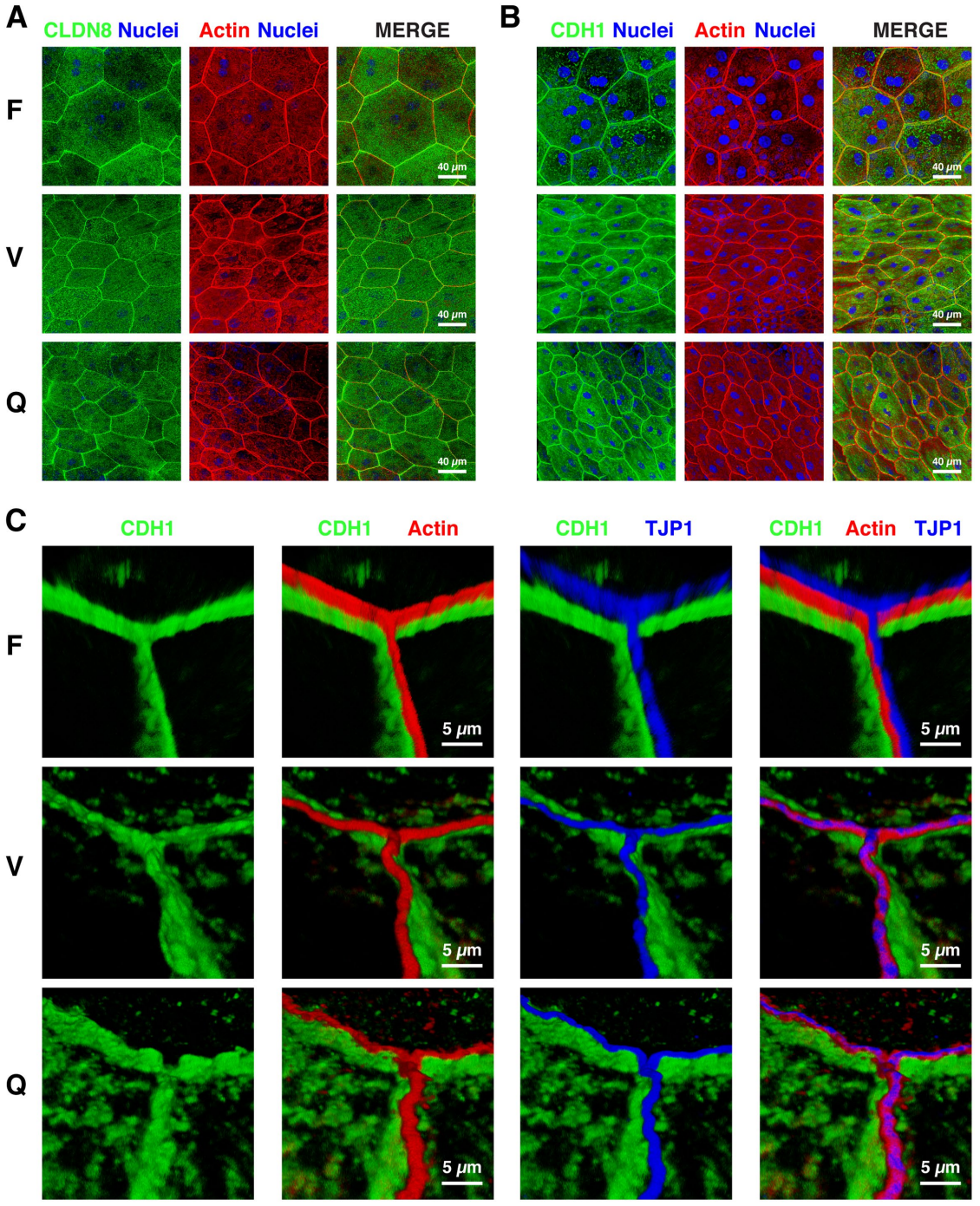

FIGURE 1: The AJR expands and contracts as a unit during bladder filling and voiding. En face view of the umbrella cell layer in whole-mount preparations of filled (F), voided (V), or quiescent (Q) rat bladders. The apical junctional complex is labeled with (A) an antibody against the transmembrane tight-junction protein CLDN8 (green) or (B) an antibody against the transmembrane adherens-junction protein CDH1 (green). F-actin is stained with rhodamine–phalloidin (red) and nuclei with To-Pro-3 (blue). Images are 3D reconstructions of confocal Z-stacks. Scale bars = 40 μm. Note that the AJR in the merged images does not appear to be completely "yellow," as the intensity of the channels is not completely matched in these large cells. (C) Higher-magnification images of the AJR in filled, voided, or quiescent bladders labeled with antibodies against the adherens-junction protein CDH1 (green) and the tight-junction protein TJP1 (blue). F-actin is labeled with rhodamine–phalloidin (red). Images are 3D reconstructions of confocal Z-stacks. Scale bars = 5 μm.

in voided and quiescent bladders, the F-actin ring was not easily resolved from the tight junction, yet remained distinct from the adherens junction. Additionally, the AJR was slightly more tortuous and rounded in appearance in the voided and quiescent bladders, whereas it was very straight and wall-like in the filled bladders (Figure 1C). In the latter studies we used antibodies against TJP1 because CLDN8 and CDH1 antibodies were both made in rabbit and because of difficulties in identifying antibodies made in

nonrabbit species that label whole-mount rat tissues. However, we previously reported that TJP1 and F-actin exhibit complete overlap in umbrella cells (Acharya *et al.*, 2004).

In the epithelial cells of the organ of Corti, the intestine, or the stomach, the AJR is organized as a highly ordered sarcomeric network (Ebrahim *et al.*, 2013). In these cells, regularly spaced puncta of NMMIIB or NMMIIC, with a periodicity of ~450 nm, are interspersed between alternating clusters of F-actin and ACTN1 (α-actinin1). This is similar to striated muscle cells, where ACTN2 (α-actinin2) and ACTN3 (α-actinin3) cross-link antiparallel F-actin filaments at the Z-line, which are engaged with muscle myosins tethered to the M-line. However, in umbrella cells, the actomyosin cytoskeleton was not obviously organized in a sarcomeric network. First, rat umbrella cells expressed MYH9 (heavy-chain NMMIIA) and MYH14 (heavy-chain NMMIIC), but not MYH10 (heavy-chain NMMIIB), which was instead expressed in the interstitial cells below the urothelium (Figure 2A and Supplemental Figure S1). NMMIIB expression in interstitial cells was confirmed by costaining with PDGFRA (platelet-derived growth factor α), which is a marker of interstitial cells in the urothelium (Supplemental Figure S1, D–F; Koh *et al.*, 2012). In the case of NMMIIA, the majority of MYH9 appeared in small punctate structures and large "aggregates" that were dispersed across the apical poles of the umbrella cells (Figure 2, A and C). When the umbrella cell AJR of filled bladders was examined at higher magnification, MYH9 close to the AJR formed very thin "railroad tracks" that overlapped with a continuous, unbroken ring of F-actin associated with the AJR (Figure 2C). Interestingly, the distribution of MYH9 was not obviously periodic, but instead appeared stochastic, and was broken into small linear foci of staining. The highly folded nature of the umbrella cell apical membrane after voiding, coupled with the thin nature of the MYH9 staining, made it more difficult to image these tissues in the voided or quiescent state. However, areas of similarly distributed MYH9 and F-actin were observed in these samples as well (Figure 2C). Although MYH14 showed a prominent apical distribution in umbrella cells (Supplemental Figure S1C), it had no obvious association with the umbrella cell AJR in either cross-section or whole-mount preparations (Supplemental Figures S1C and S2).

We also examined the distribution of ACTN4 (α-actinin4) in umbrella cells. Its association with the AJR was apparent even in relatively low-magnification images (Figure 2B). Like MYH9, ACTN4 was closely apposed to the apical F-actin ring, again forming a "railroad track" pattern on either side of adjacent cell contacts (Figure 2D). However, its localization appeared more continuous, not obviously punctate, and thicker than the fine linear elements formed by MYH9 (Figure 2D). Because ACTN4 and MYH9 antibodies were both made in rabbit, we could not colocalize MYH9 with ACTN4. We also observed that ACTN4 was associated with a network of interlocking structures that had a meshlike appearance (Figure 2D). The nature of these structures is unknown.

Taken together, our studies indicate that the actomyosin cytoskeleton of the umbrella cell AJR is organized as a nonsarcomeric network with F-actin forming a thin continuous ring, bordered on either side by ACTN4 and coincident with short linear arrays of MYH9 (NMMIIA). While voiding and filling did not impact this organization in an observable way, within the *z*-axis the F-actin ring appeared to segregate from the tight junction during filling, indicating some degree of reorganization of the AJR during the bladder cycle.

AJR expansion depends on the actin cytoskeleton

In the above studies, we allowed urethane-anesthetized rats to fill their bladders spontaneously; however, to explore the changes in the AJR accompanying bladder filling and voiding in greater detail, we needed an approach that would allow us to incorporate pharmacological treatments during the bladder cycle. Thus, we transurethrally catheterized the anesthetized rats, which allowed us to fill their bladders to a specified volume over a given period of time using a syringe pump in a controlled manner. To assess the impact that filling had on the continuity of the urothelium and AJR perimeter per umbrella cell, we filled bladders to a volume of 500 µl (the approximate volume achieved during spontaneous filling after 2.5 h; Carattino *et al.*, 2013), 1000 µl, or 1500 µl. Using the F-actin ring as a surrogate for the AJR, we quantified the length of the umbrella cell AJR perimeter (µm). Compared with unfilled control bladders (0 µl), filled bladders exhibited an apparent volume-dependent increase in the AJR perimeter of umbrella cells (Figure 3, A–D). The increase in AJR perimeter was not linear, but instead fit a single exponential ($R^2 = 0.91$) with a $V_{1/2}$ of 663.6 µl (95% CI = 304–1327 µl, $n = 3$), indicating that AJR approached its maximum size by 1500 µl (Figure 3E). As 500 µl was close to the measured $V_{1/2}$, we used this volume in our subsequent analyses.

To assess the actin requirements for AJR expansion, we preincubated the bladder by introducing a small volume (50 µl) of the actin-disrupting agent cytochalasin D (CytoD; 25 µg/ml) into the bladder and then allowed the bladder to remain in a quiescent state for 60 min. Subsequently, the bladder was filled to a final volume of 500 µl in the continued presence of the drug. Under these conditions, CytoD had a modest but significant inhibitory effect on filling-induced increases in AJR perimeter (Figure 4, A, B, and G). In contrast, and relative to dimethylsulfoxide (DMSO)-treated control samples, preincubation with CytoD in the absence of subsequent filling had no obvious effect on the AJR perimeter (Q = 169 ± 10 µm vs. Q + CytoD = 178 ± 3 µm; $p > 0.05$). As we reported previously, the concentration of CytoD used in our studies (25 µg/ml) caused the cytoplasmic accumulation of "focal aggregates" of F-actin (see arrows in Figure 4B), but did not obviously disrupt the AJR-associated F-actin cytoskeleton or the continuity of the umbrella cell layer (Khandelwal *et al.*, 2010). We also measured the effects of CytoD on filled bladders not preincubated with this drug before analysis (Figure 4, C and G). In this case, the AJR perimeter was not significantly different from that for filled bladders, indicating that preincubation was necessary to observe the effects of this drug.

Because we observed that general disruption of the F-actin cytoskeleton with CytoD prevented the complete expansion of the AJR, we investigated what types of actin polymerization might be involved in this process. Both ARP2/3 and formins are involved in the formation and maintenance of the functional AJR (Park *et al.*, 2013; Zhou *et al.*, 2013). Therefore, we incubated bladders with either 100 µM CK869, an ARP2/3 inhibitor (Nolen *et al.*, 2009), or 50 µM SMIFH2, a formin polymerization inhibitor (Rizvi *et al.*, 2009), before and during filling. Whereas treatment with SMIFH2 before filling caused a significant decrease in the AJR perimeter relative to that for DMSO-filled control bladders, CK869 treatment did not significantly affect AJR expansion (Table 1). Because CDC42 can act upstream of formins (Ma *et al.*, 1998; Vogler *et al.*, 2014), we also examined the effects of 25 µM ML141, a CDC42 inhibitor (Surviladze *et al.*, 2010). However, ML141 treatment did not significantly affect AJR expansion in response to bladder filling.

In many cells, the long, tangentially oriented F-actin filaments within the AJR are cross-linked by NMMIIA molecules to form a contractile unit (Schwayer *et al.*, 2016). To examine whether NMMII contraction played a role in AJR expansion during bladder filling, we preincubated bladders with blebbistatin (Bleb; 10 µM), which specifically inhibits the ATPase activity of the myosin heavy chains

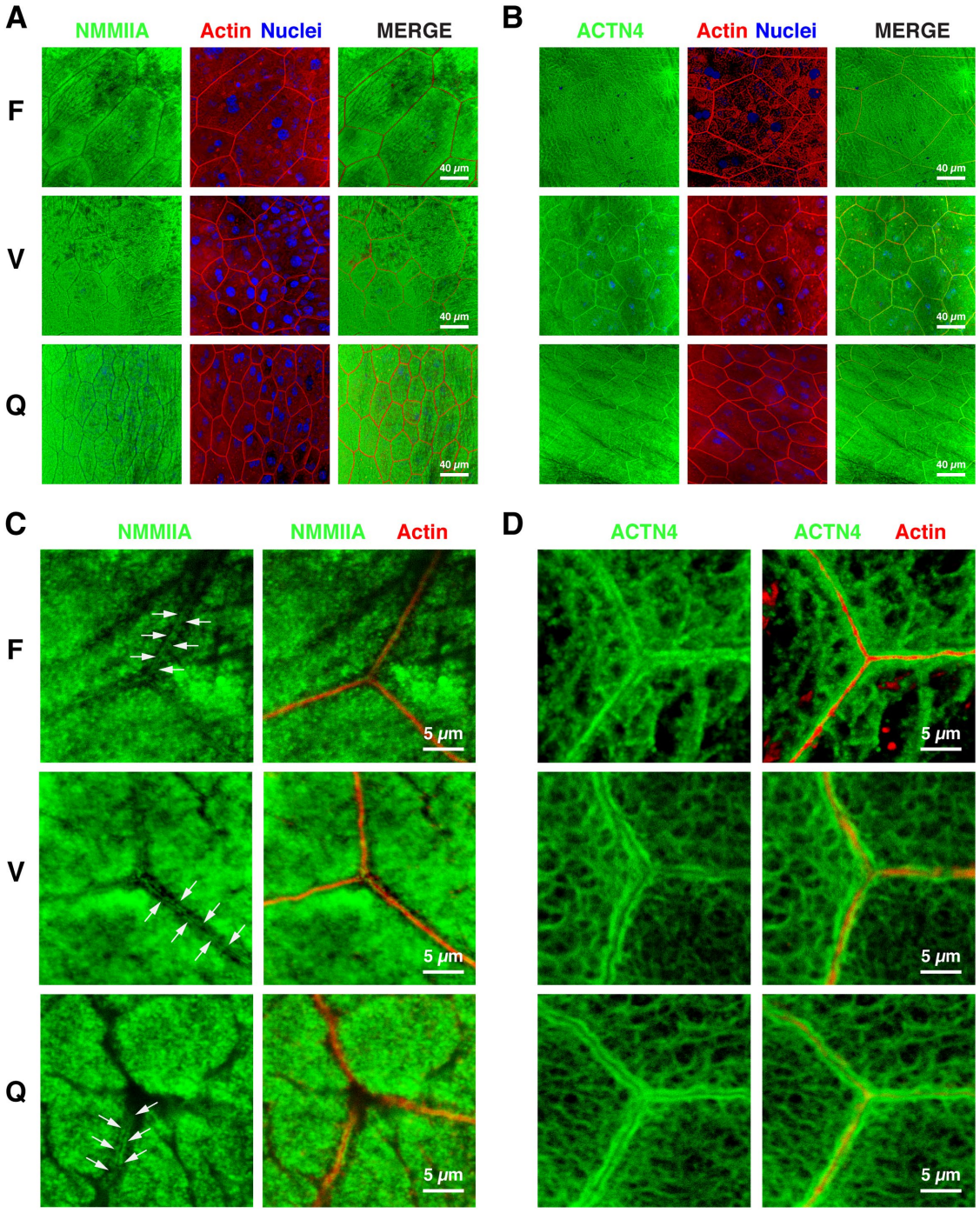

FIGURE 2: The junctional actomyosin cytoskeleton expands and contracts with the apical junctional complex during bladder filling and voiding. En face view of the umbrella cell layer in whole-mount preparations of filled (F), voided (V), or quiescent (Q) rat bladders. The tissue is labeled with (A) an antibody against NMMIIA (MYH9 subunit; green) or (B) an antibody against ACTN4 (green). F-actin is stained with rhodamine–phalloidin (red) and nuclei with To-Pro-3 (blue). Images are 3D projections of confocal Z-stacks. Scale bars = 40 μm. (C, D) Higher-magnification images of the AJR in filled (F), voided (V), or quiescent (Q) bladders labeled with antibodies against (C) NMMIIA (MYH9 subunit; green; arrows indicate "railroad track" distribution of NMMIIA) or (D) ACTN4 (green). F-actin is labeled with rhodamine–phalloidin (red). Images are 3D projections of confocal Z-stacks. Scale bars = 5 μm.

associated with vertebrate NMMIIA, NMMIIB, and NMMIIC complexes (Zhang *et al.*, 2017). However, there was no significant effect on filling-induced AJR expansion after Bleb treatment (Figure 4G). Furthermore, bladders preincubated with Bleb, but left in a quiescent state, showed no change in AJR perimeter relative to that of untreated control bladders (Q = 169 ± 10 μm vs. Q + Bleb = 166 ± 0.4 μm; $p > 0.05$). As further evidence that NMMII may not play an active role during bladder filling, we preincubated bladders with 100 nM GSK269962, a selective ROCK inhibitor, which should prevent ROCK-dependent activation of NMMII (Doe *et al.*, 2007).

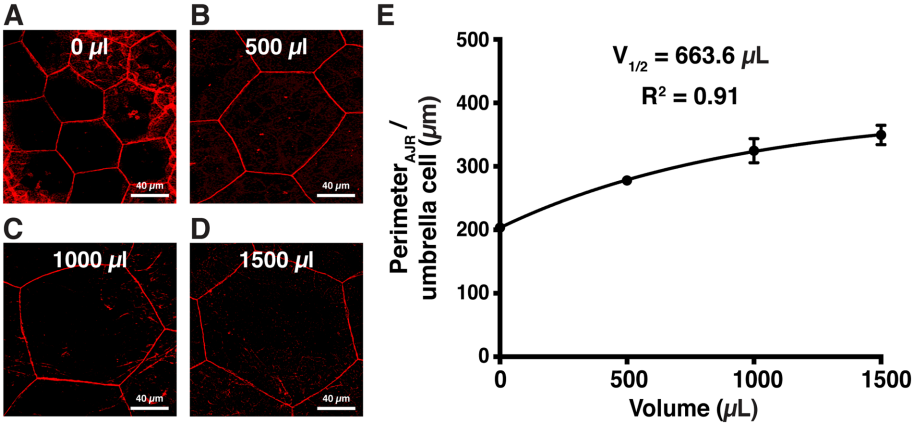

FIGURE 3: Effect of filling on average perimeter$_{AJR}$ per umbrella cell. En face view of the umbrella cell layer in whole-mount preparations of rat bladders (A) left quiescent (0 µl) or filled with (B) 500, (C) 1000, or (D) 1500 µl of Kreb's buffer over 45 min (n = 3 for each group). F-actin is labeled with rhodamine–phalloidin (red). Images are 3D reconstructions of confocal Z-stacks. In some panels, the underlying intermediate cell layers are visible, but only the junctions associated with the uppermost umbrella cell layer were quantified. Scale bars = 40 µm. (E) Average perimeter$_{AJR}$ per umbrella cell (mean ± SEM; n = 3).

Again, GSK269962 did not affect expansion of the AJR (Table 1). Overall, our data indicate that active formin-mediated actin polymerization, but not NMMII contraction, is required for the expansion of the umbrella cell AJR during bladder filling.

RAB13-dependent trafficking events are required for expansion of the umbrella cell AJR during bladder filling

Many membrane trafficking events, including exocytosis and endocytosis, are actin-dependent (Valentijn *et al.*, 1999; Apodaca, 2001a, 2002; Croise *et al.*, 2014). In the case of umbrella cells, the apical exocytosis stimulated by bladder filling is actin-dependent (Lewis and de Moura, 1982; Apodaca, 2001b; Truschel *et al.*, 2002; Yu *et al.*, 2009), as is voiding-induced apical endocytosis (Khandelwal *et al.*, 2010). This prompted us to determine whether exocytosis is required for filling-induced expansion of the AJR. As a general inhibitor of the biosynthetic pathway, we preincubated bladders with brefeldin A (BfA; 5 µg/ml), which impairs exocytosis by preventing the exit of proteins from the Golgi (Klausner *et al.*, 1992). Compared with control bladders, BfA-treated bladders were unable to fully expand their AJRs (Figure 4, A, D, and H) and exhibited a significant decrease in AJR perimeter relative to that of control bladders (Figure 5H). However, in the absence of preincubation, the AJRs of BfA-treated umbrella cells were able to expand to a perimeter similar to that measured in control filled bladders (Figure 4, E and H). We also preincubated bladders with the protein synthesis inhibitor cycloheximide (Schneider-Poetsch *et al.*, 2010; CHX, 100 µg/ml), which also significantly inhibited the increase in AJR perimeter that normally accompanies bladder filling (Supplemental Figure S3).

To more specifically target the exocytic machinery that could be involved in the expansion of the AJR, we used adenoviral transduction to express dominant-negative (DN) mutants of RAB8A, RAB11A, and RAB13, or GFP alone as a control. A critical step in this approach is brief treatment with *N*-dodecyl-β-D-maltoside, which makes the umbrella cells permissive for adenoviral infection (Ramesh *et al.*, 2004; Khandelwal *et al.*, 2008). While this treatment has no effect on the transepithelial resistance of the urothelium or the expression and distribution of differentiation markers (Khandelwal *et al.*, 2010; Carattino *et al.*, 2013), it does cause the umbrella cells to become smaller in perimeter, a phenotype that reverses slowly over several days. Nonetheless, these cells were still capable of expanding and contracting their AJRs in response to filling and voiding. We first explored the impact of expressing DN-RAB8A-GFP or DN-RAB11A-GFP, as these mutant GTPases inhibit the pathways for apical exocytosis that expand the umbrella cell apical surface area in response to filling (Khandelwal *et al.*, 2008, 2013). To ensure that we quantified effects only in transduced umbrella cells, we measured the perimeter of AJR per umbrella cell in GFP-positive cells. Relative to GFP alone, expression of either DN-RAB8A-GFP or DN-RAB11A-GFP did not significantly affect the perimeter of AJR per umbrella cell in filled bladders (Figure 5, A–C and E). Interestingly, umbrella cells transduced with DN-RAB8A-GFP exhibited profound changes in the morphology of their AJRs, which became highly convoluted, even in filled bladders (see arrowheads in Figure 5B). Of the known Rabs, RAB13 is the one most often associated with trafficking events that occur at the tight junction (Marzesco *et al.*, 2002; Marzesco and Zahraoui, 2005; Kohler *et al.*, 2004; Yamamura *et al.*, 2008). We confirmed by Western blot and immunofluorescence that rat umbrella cells expressed RAB13 (Supplemental Figure S4). Whereas expression of DN-RAB8A-GFP or DN-RAB11A-GFP had no significant effect on expansion of the AJR, expression of DN-RAB13A-GFP resulted in a significant decrease in AJR perimeter relative to that of GFP-expressing umbrella cells in filled bladders (Figure 5, A, D, and E). We compared the expression levels of exogenously expressed DN-Rab mutants with those of their endogenous counterparts and confirmed that relative expression levels were similar and thus could not account for the observed inhibitory effect of DN-RAB13 versus the other Rabs tested (Supplemental Figure S5). Collectively, these data indicate that expansion of the AJR requires new protein synthesis and RAB13-dependent exocytosis.

Contraction of the AJR requires actin, NMMII, RHOA, and dynamin-dependent endocytosis

We next explored the requirements for AJR contraction during voiding, focusing on the role of the actomyosin cytoskeleton in the events. As noted in Figure 4G, if the bladder was filled in the presence of CytoD, but without preincubation, there was no significant effect on AJR expansion. However, when this treatment protocol was followed by voiding, CytoD reduced the voiding-induced contraction of the AJR (Figure 6, A, B, and G). Thus, the actin cytoskeleton is involved in both the expansion and the contraction of the umbrella cell AJR during bladder filling and voiding. To examine whether there was also a role for NMMII in AJR contraction, we preincubated bladders with Bleb, filled the bladders, and then induced voiding. Under these conditions, Bleb impaired the contraction of the AJR, resulting in a significant increase in AJR perimeter relative to control voided bladders (Figure 6, A, C, and G). An upstream regulator of NMMIIA is RHOA (Amano *et al.*, 1996). Thus, we also tested whether expression of DN-RHOA-GFP impacted AJR contraction. We observed that expression of DN-RHOA-GFP caused a moderate, but significant, increase in AJR perimeter per umbrella cell versus that of

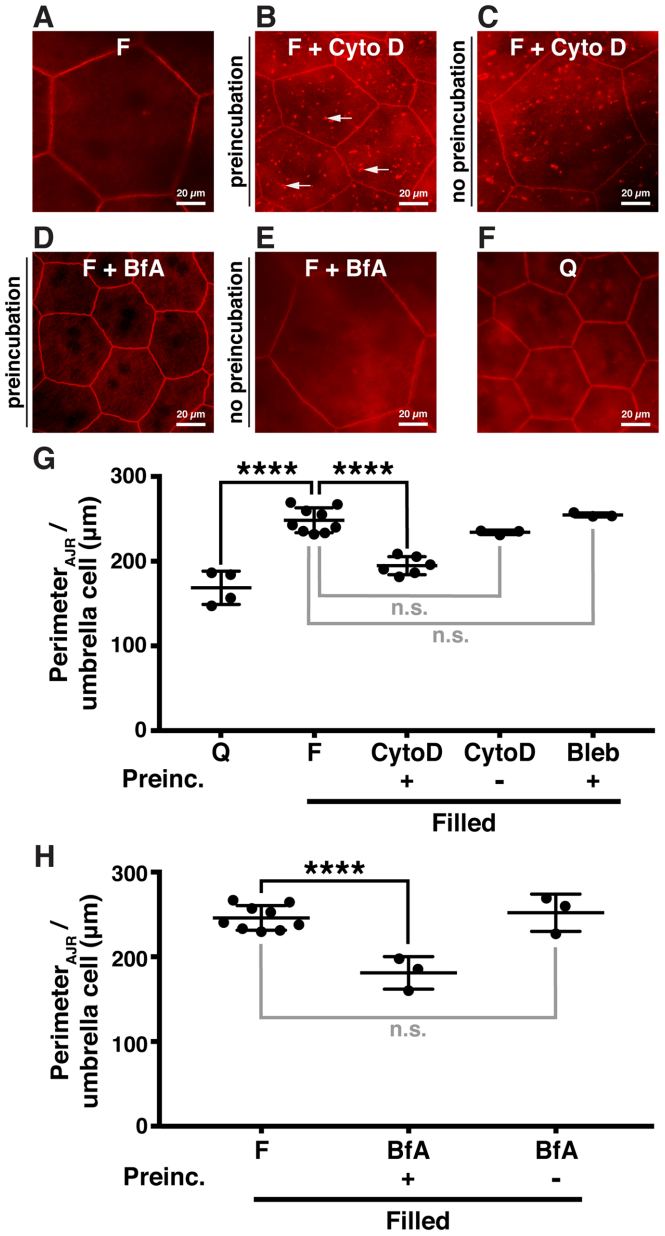

FIGURE 4: F-actin disruption or inhibition of exocytosis impairs AJR expansion during bladder filling. En face view of the umbrella cell layer in whole-mount preparations of rat bladders that were treated as follows: (A) preincubated with Kreb's buffer + 0.1% DMSO for 1 h, and filled in the presence of DMSO (F; control); (B) preincubated for 1 h with 25 μg/ml CytoD and then filled in the presence of the drug; (C) not preincubated, but filled in the presence of 25 μg/ml CytoD; (D) preincubated for 1 h with 5 μg/ml BfA and then filled in the presence of the drug; (E) not preincubated, but filled in the presence of 5 μg/ml BfA; or (F) catheterized but never allowed to fill (Q). F-actin is labeled with rhodamine–phalloidin (red). The "focal aggregates" of F-actin that resulted from CytoD treatment (B) are indicated with arrows. Images were acquired using a wide-field microscope equipped with a digital camera. Scale bars = 20 μm. (G, H) Average perimeter$_{AJR}$ per umbrella cell in (G) quiescent bladders (Q; $n = 4$); control filled bladders preincubated with DMSO, and then filled in the presence of DMSO (F; $n = 9$); bladders preincubated with CytoD, and then filled in the presence of the drug ($n = 6$); bladders not preincubated, but filled in the presence of CytoD ($n = 3$); bladders preincubated with Bleb, and then filled in the presence of the drug ($n = 3$); and in (H) control filled bladders preincubated with DMSO and then filled in the presence of DMSO (F; $n = 9$); bladders preincubated with BfA and then filled in the presence of the drug ($n = 3$); bladders not preincubated, but filled in the presence of BfA ($n = 3$). Control data for filled bladders are reproduced from G. Values are mean ± SEM. Data were analyzed using ANOVA and p values ≤ 0.05 were considered significant, with **** denoting a p value ≤ 0.0001.

umbrella cells transduced with GFP (Figure 7, A, B, and D). We also confirmed that DN-RHOA-GFP had no effect on expansion of the AJR (Figure 7D). Taken together, these data indicate that contraction of the actomyosin cytoskeleton is required for the constriction of the umbrella cell AJR upon bladder voiding.

Like exocytosis, endocytosis is also intimately linked to the actomyosin cytoskeleton (Apodaca, 2001a). For example, we previously showed that voiding-induced apical endocytosis in umbrella cells is dependent on RHOA and actin, as well as DNM2 (Truschel *et al.*, 2002; Khandelwal *et al.*, 2010). This indicated to us that contraction of the AJR may also depend on endocytosis. To examine this possibility, we preincubated bladders with 30 μM Pitstop2, which was originally identified in a screen for inhibitors of clathrin-mediated endocytosis (von Kleist *et al.*, 2011), but was later shown to be a general inhibitor of clathrin-dependent and -independent endocytosis (Dutta *et al.*, 2012). While preincubation with Pitstop2 had no effect on filling-induced expansion of the AJR, it impaired contraction of the AJR, resulting in an increase in AJR perimeter (Figure 6, D–F and H). We also determined whether AJR contraction was dependent on dynamin, a GTPase required for clathrin-dependent and -independent forms of endocytosis (Mayor *et al.*, 2014; Kaksonen and Roux, 2018). While we previously reported that umbrella cells express DNM2 (Khandelwal *et al.*, 2010), we chose to use a DN mutant of DNM1 (HA-tagged DNM1-K44A) because of reports that DNM2 can trigger apoptosis when overexpressed (Soulet *et al.*, 2006). Expression of DN-DNM1-HA had no impact on the expansion of the AJR (Figure 7D); however, it caused a significant increase in AJR perimeter per umbrella cell in voided bladders as compared with voided bladders expressing GFP (Figure 7, A, C, and D). Taken as a whole, these data indicate that the contraction of the AJR during bladder voiding is dependent not only on the actomyosin cytoskeleton, but on dynamin-dependent endocytosis as well.

DISCUSSION

While many previous studies have focused on the internal forces generated by the actomyosin cytoskeleton on mature, stable junctions or on the remodeling of junctions during development, there is limited understanding of how the AJR responds to the external forces that occur during normal physiological events. In the case of umbrella cells, we previously reported that they expanded and contracted their AJRs as the bladder underwent cycles of filling and voiding (Carattino *et al.*, 2013). How this is accomplished is unknown, but it is unlikely to result from simple folding and unfolding of the AJR, as even at the ultrastructural level there is little evidence of AJR pleating (Carattino *et al.*, 2013). Instead, our current studies indicate that expansion of the umbrella cell AJR, which has a nonsarcomeric organization, requires actin polymerization and membrane-trafficking events, likely exocytosis, while constriction of the umbrella cell AJR requires NMMII-dependent contraction coupled with endocytosis. The importance of these findings is discussed.

Experimental group	*n*	Function	Conc.	P_{AJR}/UC (μm) ± SEM
Full DMSO control	4		0.1%	215 ± 16
CK869	4	ARP2/3 complex inhibitor	100 μM	176 ± 9
Full DMSO control	6		0.1%	236 ± 12
SMIFH2	6	Formin FH2 domain inhibitor	50 μM	180 ± 16*
Full DMSO control	4		0.1%	204 ± 5
ML141	4	CDC42 inhibitor	25 μM	202 ± 10
Full DMSO control	3		0.1%	196 ± 31
GSK 269962	4	ROCK inhibitor	100 nM	203 ± 7

Rat bladders were preincubated with the indicated pharmacological agent for 1 h prior to filling. Average $perimeter_{AJR}$ per umbrella cell (P_{AJR}/UC) of experimental bladders was compared with that of paired control bladders (mean ± SEM). A paired two-tailed *t* test was performed and *p* values ≤0.05 were considered significant, with a * denoting a *p* value ≤ 0.05.

TABLE 1. Effects of pharmacological inhibitors on AJR expansion during bladder filling.

Organization and dynamics of the AJR-associated actomyosin cytoskeleton in umbrella cells

While the AJR and its components have been known for decades (Farquhar and Palade, 1963), the past few years have revealed important insights into the details of its organization, particularly that of the associated actomyosin ring. In the epithelial cells that line the organ of Corti, the intestine, and the stomach, the actomyosin ring forms a sarcomeric belt composed of bipolar NMMIIB/C filaments, arranged in punctae, that are periodically interspersed between punctae of ACTN1-tethered actin filaments—an organization that would be ideal to promote contraction (Ebrahim *et al.*, 2013) (Supplemental Figure S7). In contrast, in *Caenorhabditis elegans*, the actomyosin cytoskeleton of the hypodermis is organized at right angles to the apical junctions (Costa *et al.*, 1998), and in cultured Madin–Darby canine kidney (MDCK) cells, punctate NMMIIB staining overlaps considerably with a continuous ring of F-actin at the AJR (Fanning *et al.*, 2012). Interestingly, when MDCK cells are depleted of TJP1/2, the bicellular junctions become more linear, the F-actin staining becomes more prominent, and NMMIIB assumes a periodic distribution, somewhat like that observed in cells with a sarcomeric AJR (Fanning *et al.*, 2012).

In the case of umbrella cells, our studies indicate that the F-actin ring is continuous, and is likely composed of long, formin-generated cables of actin filaments. Consistent with this possibility, we observe that expansion of the umbrella cell AJR is sensitive to an inhibitor of formin-dependent actin polymerization. Interestingly, it has been shown that the formin mDia1 is mechanosensitive, and pulling force applied to individual actin filaments is sufficient to promote an increased rate of filament elongation. Additionally, mDia1 is able to respond to an opposing pulling force by promoting barbed end polymerization thereby generating mechanical tension on actin filaments (Jegou *et al.*, 2013). Thus, formins could potentially both sense increased tension generated by bladder filling and respond to this increased force by generating tension on cortical actin filaments. We also tested the effects of the ARP2/3 inhibitor CK869, but we observed no significant impact on AJR expansion after treatment with this drug. However, it is possible that other, more targeted inhibitors of ARP2/3 may reveal a requirement for this form of actin polymerization in future studies. We also observed that NMMIIA forms short linear structures that, similarly to MDCK cells, overlap with the F-actin ring. ACTN4 also forms a ring on either side of the F-actin ring, but ACTN4 formed thicker, more continuous tracts than those formed by NMMIIA. While we were unable to resolve changes in the actomyosin network in filled bladders versus those fixed 5 min after voiding, it is possible that during the actual voiding event F-actin, ACTN4, and NMMIIA undergo a rapid and reversible rearrangement, promoting contraction. Intriguingly, in the *Drosophila* pupal wing, junctional expansion requires the down-regulation of NMMII activity (Bardet *et al.*, 2013). This could explain why inhibition of NMMII with Bleb has no effect on AJR expansion during bladder filling, but voiding-triggered AJR contraction is sensitive to Bleb treatment.

Another difference in the AJR of filled versus voided bladders is the position of the F-actin ring with respect to the tight junction in the Z-axis. While the F-actin ring is easily resolved from the tight junction in filled bladders, this is not true of voided (or quiescent) bladders. Additionally, the AJR appears very narrow and tall in filled bladders, while it looks shorter and more rounded in voided and quiescent bladders. Whether these differences reflect changes in the folding of the cells or molecular rearrangements of the junctional complex is difficult to determine in these highly deformable cells and using the techniques we employed. In this regard, electron microscopy, similar to that performed by Efimova and Svitkina (Efimova and Svitkina, 2018), is likely to be highly revealing if it can be adapted to non–coverslip grown umbrella cells. Coupled with our previous observations that filling increases paracellular conductance of ions without altering barrier function (Carattino *et al.*, 2013), our current studies indicate that the filling/voiding cycle not only impacts the function of the tight junction, it also apparently impacts the organization of the AJR.

Expansion of the umbrella cell AJR

Other than cell intercalation and cell extension in *Drosophila* (Butler *et al.*, 2009; Kong *et al.*, 2017), there are few reports of AJR expansion, particularly in response to external mechanical stimuli. Intriguingly, cultured endothelial cells increase the area of their adherens junction in response to applied stretch (Liu *et al.*, 2010), but whether they also increase the perimeter of their AJR around each cell is unknown. In the case of the umbrella cell, we report that expansion of the AJR depends not only on the actin cytoskeleton, but also on membrane trafficking events, likely exocytosis. In support of this latter possibility, we observe that AJR expansion is inhibited by treatment with BfA. This drug is a general inhibitor of biosynthetic traffic along the ER-to-Golgi route (Klausner *et al.*, 1992), but can also impact cargo sorting events in endosomes (Wang *et al.*, 2001). The inhibition of AJR expansion by CHX is consistent with the possibility that biosynthetic traffic, possibly of newly synthesized junctional

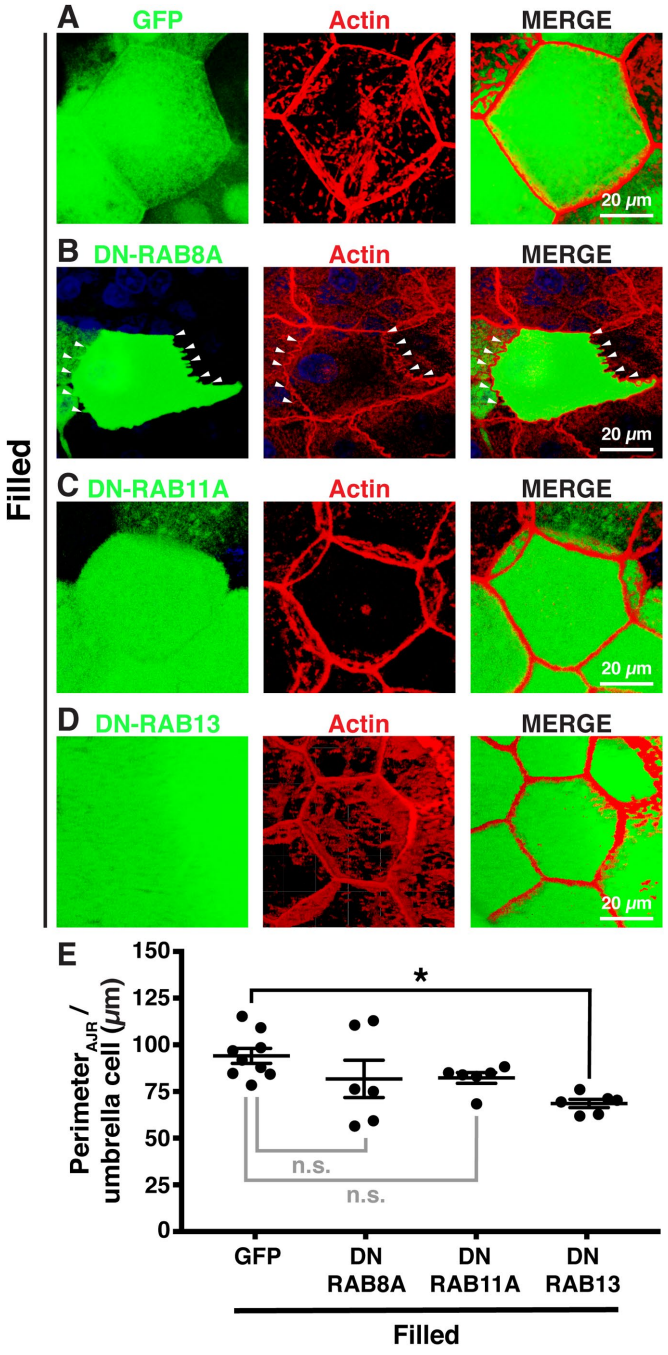

FIGURE 5: Expression of DN-RAB13-GFP impairs AJR expansion during bladder filling. En face view of the umbrella cell layer in whole-mount filled rat bladders transduced with adenoviruses encoding (A) GFP (control), (B) DN-RAB8A-GFP (arrowheads indicate altered AJR morphology in cells expressing this protein), (C) DN-RAB11A-GFP, or (D) DN-RAB13-GFP. F-actin was labeled with rhodamine–phalloidin (red). Images are 3D reconstructions of confocal Z-stacks. Scale bars = 20 μm. (E) Average perimeter$_{AJR}$ per umbrella cell in bladders transduced with GFP ($n = 9$), DN-RAB8A-GFP ($n = 6$), DN-RAB11A-GFP ($n = 6$), or DN-RAB13-GFP ($n = 6$). Values are mean ± SEM. Data were analyzed using ANOVA, with * denoting a p value ≤ 0.05.

components, is involved; however, it is feasible that CHX is instead preventing the synthesis of a regulatory protein(s) that is necessary for AJR expansion to occur.

We also explored the role of trafficking pathways modulated by RAB11A, RAB8A, and RAB13 in AJR expansion. Our investigation was driven in part by a long-standing interest in the abundant population of subapical discoidal and/or fusiform vesicles that undergo regulated exocytosis in response to bladder filling (Apodaca, 2001b; Truschel *et al.*, 2002). Our previous studies, and those of others, established that these events were dependent on a RAB11A–RAB8A–MYO5B network (Khandelwal *et al.*, 2008, 2013), as well as RAB27B (Watson *et al.*, 2001; Chen *et al.*, 2003; Gallo *et al.*, 2018). Although one would predict that a mechanism exists that coordinates the large increase in apical surface area with expansion of the AJR, in our current analysis we observe no significant role for RAB11A or RAB8A in AJR expansion. Instead, the expansion of the AJR is dependent on RAB13, a well-described regulator of tight junction protein trafficking (Marzesco *et al.*, 2002; Marzesco and Zahraoui, 2005; Kohler *et al.*, 2004; Yamamura *et al.*, 2008). Interestingly, in cultured epithelial cells, knockdown of RAB13 specifically reduces the trafficking of CLDN1 (claudin-1) and OCLN (occludin) to the surface, but not CDH1 (Yamamura *et al.*, 2008), whereas RAB8 (Yamamura *et al.*, 2008) and RAB11A (Lock and Stow, 2005; Desclozeaux *et al.*, 2008; Chung *et al.*, 2014; Woichansky *et al.*, 2016) are primarily associated with the membrane trafficking of cadherins. These findings are at odds with our analysis, as all components of the umbrella cell AJR appear to move synchronously. These differences may reflect cell-specific RAB function. For example, in umbrella cells RAB11A primarily operates along the secretory pathway (Khandelwal *et al.*, 2008, 2013), whereas in many other cell types RAB11A functions within the endocytic system (Welz *et al.*, 2014). Another possible explanation for the observed differences is that we were exploring responses to external mechanical forces, whereas the studies in cultured cells examined junction dynamics when extracellular Ca^{2+} was depleted and then replenished (Yamamura *et al.*, 2008).

Contraction of the umbrella cell AJR

While the umbrella cell AJR expands during filling, it contracts rapidly during voiding. How quickly this occurs is unclear, although we know from studies of voiding-induced endocytosis in ex vivo preparations of bladder that apical membrane can be recovered in on the order of several seconds (Khandelwal *et al.*, 2010). Presumably, the same is true of the AJR. Like expansion of the AJR, its contraction also depends on the actin cytoskeleton and membrane traffic; however, the specific molecules and pathways involved are different. During voiding, contraction of the AJR likely depends on the actin cytoskeleton and NMMII contraction, as treatment with CytoD or Bleb, an inhibitor of NMMIIA, NMMIIB, and NMMIIC (Allingham *et al.*, 2005; Zhang *et al.*, 2017), impairs AJR contraction. The lack of expression of NMMIIB in umbrella cells would indicate that either NMMIIA or NMIIC is chiefly responsible for this contraction. However, the accumulation of NMMIIA on either side of the AJR, forming "railroad tracks," indicates that it may the primary regulator of AJR contraction. We also noted that AJR contraction, but not its expansion, is dependent on RHOA, an important regulator of both actomyosin contraction upstream of NMMIIA and membrane internalization, including voiding-induced apical endocytosis in umbrella cells (Lamaze *et al.*, 2001; Doherty and McMahon, 2009; Khandelwal *et al.*, 2010; Arnold *et al.*, 2017).

Consistent with analyses of dorsal closure and cell intercalation in *Drosophila* (Levayer *et al.*, 2011; Mateus *et al.*, 2011), as well as the apical constriction that accompanies *Xenopus* gastrulation (Lee and Harland, 2010), we observe that endocytosis plays a critical role

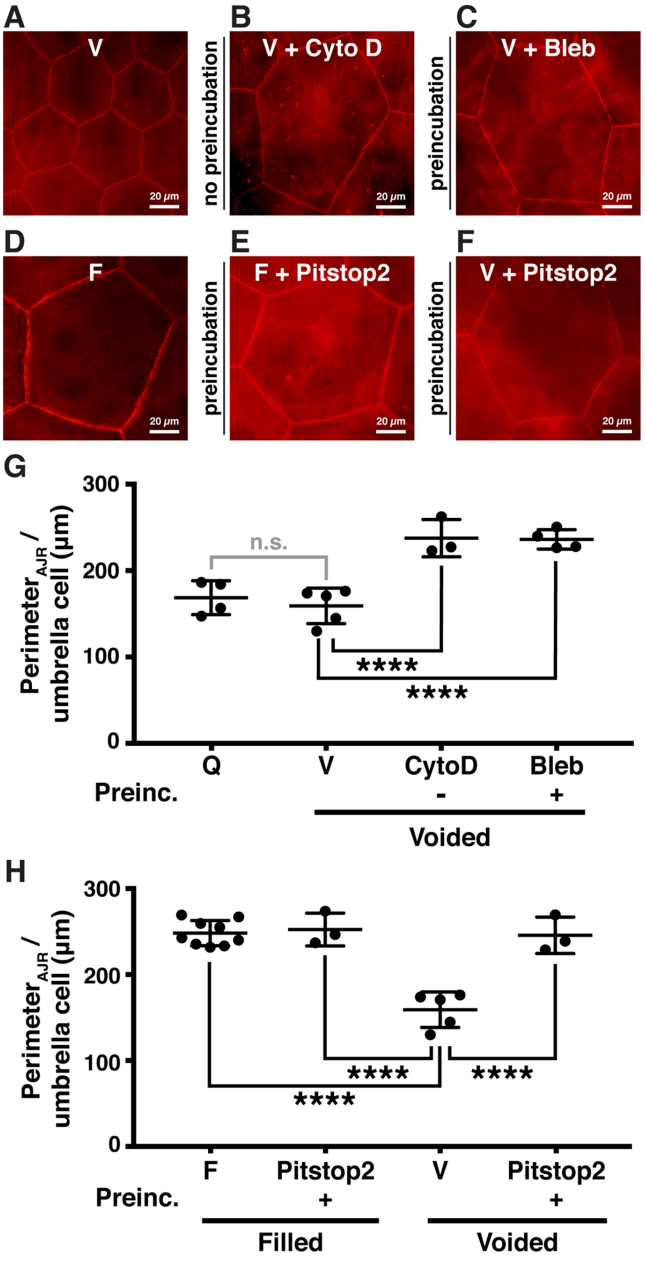

FIGURE 6: Disruption of the actin cytoskeleton, inhibition of NMMIIA contractility, or inhibition of endocytosis impairs AJR contraction during bladder voiding. En face view of the umbrella cell layer of whole-mount rat bladders that were (A) preincubated with Kreb's buffer + 0.1% DMSO for 1 h, filled in the presence of DMSO, and then voided (V; control); (B) not preincubated, but filled in the presence of 25 μg/ml CytoD and then voided; (C) preincubated for 1 h with 10 μM Bleb, filled in the presence of the drug, and then voided; (D) preincubated with Kreb's buffer + 0.1% DMSO for 1 h and filled in the presence of DMSO (F; control); (E) preincubated for 1 h with 30 μM Pitstop2 and filled in the presence of the drug; or (F) preincubated for 1 h with 30 μM Pitstop2, filled in the presence of the drug, and then voided. F-actin was stained with rhodamine–phalloidin (red). Images were acquired using a wide-field microscope fitted with a digital camera. Scale bars = 20 μm. (G, H) Average perimeter$_{AJR}$ per umbrella cell in (G) quiescent bladders (Q; $n = 4$); control voided bladders preincubated with DMSO, filled in the presence of DMSO, and then voided (V; $n = 5$); bladders not preincubated, but filled in the presence of 25 μg/ml CytoD, and then voided ($n = 3$); bladders preincubated for 1 h with 10 μM Bleb, filled in the presence of the drug, and then voided ($n = 4$); and in (H) control filled bladders preincubated with DMSO and filled in the presence of DMSO (F; $n = 9$); bladders preincubated with Pitstop2, and filled in the presence of the drug ($n = 3$); control voided bladders preincubated with DMSO, filled in the presence of DMSO, and then voided (V; $n = 5$); bladders preincubated with Pitstop2, filled in the presence of the drug, and then voided. Control data from quiescent bladders are reproduced from Figure 4G, control data from filled bladders are reproduced from Figure 4G, and control data from voided bladders are reproduced from G here. Values are mean ± SEM. Data were analyzed using ANOVA and p values ≤ 0.05 were considered significant, with **** denoting a p value ≤ 0.0001.

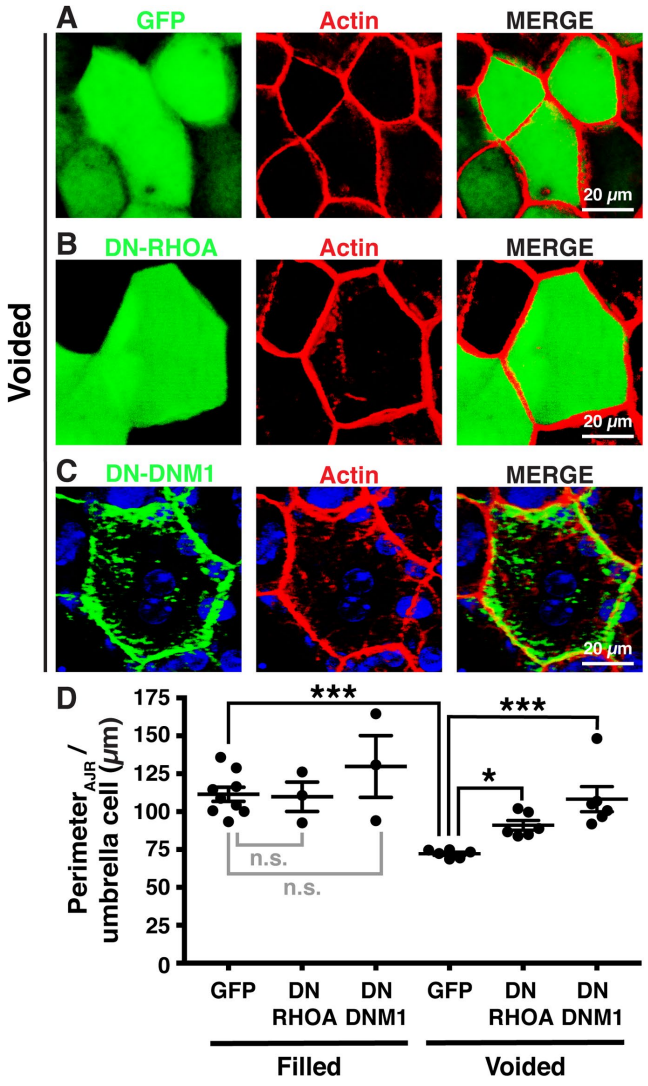

FIGURE 7: Expression of DN-RHOA or DN-DNM1 impairs AJR contraction during bladder voiding. En face view of the umbrella cell layer of whole-mount voided rat bladders transduced with adenoviruses encoding (A) GFP (control), (B) DN-RHOA-GFP, or (C) DN-DNM1-HA. F-actin was labeled with rhodamine-phalloidin (red) and nuclei with To-Pro-3 (blue). Images are 3D reconstructions of confocal Z-stacks. Scale bars = 20 μm. (D) Average perimeter$_{AJR}$ per umbrella cell in filled bladders transduced with GFP ($n = 9$), DN-RHOA-GFP ($n = 3$), or DN-DNM1-HA ($n = 3$), or voided bladders transduced with GFP ($n = 6$), DN-RHOA-GFP ($n = 6$), or DN-DNM1-HA ($n = 6$). Control data from GFP filled bladders are reproduced from Figure 5E. Values are mean ± SEM. Data were analyzed using ANOVA and p values ≤0.05 were considered significant, with *** denoting a p value ≤ 0.001.

in the contraction of the umbrella cell AJR. Here, we observe that Pitstop2 and expression of DN-DNM1 both inhibit AJR contraction. Intriguingly, we previously reported that TJP1 and F-actin are associated at the cytoplasmic face of endocytic structures, which we called "peripheral junction-associated apical endosomes" (PJAEs; Khandelwal *et al.*, 2010). PJAEs accumulated near the AJR immediately upon voiding, indicating that the AJR may be a site for nucleation of endocytic structures. If other components of the AJR, including claudins, CDH1, or NMMIIA are also localized to these structures is unknown. We also previously reported that voiding-induced endocytosis was triggered by β_1 integrins and their downstream pathways (Khandelwal *et al.*, 2010). Again, it will be interesting to determine whether similar pathways are involved in contraction of the umbrella cell AJR.

Summary

Under normal physiological conditions, epithelial cells are exposed to mechanical forces as gases, fluids, and solids pass over their surfaces and push against them. How these external mechanical forces affect AJR activity (e.g., adhesion and permeability), remodeling, and stability has only received passing attention. Our studies demonstrate that as tension within the bladder wall builds during filling, the umbrella cell actively dissipates these forces by expanding its AJR, which depends on actin dynamics and RAB13-mediated trafficking events. Upon voiding, the decrease in wall tension likely triggers NMMIIA-dependent actomyosin contraction, which along with endocytosis returns the umbrella cell AJR back to its pretension state, ready for the next cycle of filling (Figure 8).

MATERIALS AND METHODS

Animals

Urinary bladders were obtained from female Sprague–Dawley rats (250–300 g; Envigo, Harlan Laboratories, Frederick, MD). Following perfusion fixation (see below), rats were killed by inhalation of 100% vol/vol CO_2 and death was confirmed by a thoracotomy. All animal studies were performed in accordance with relevant guidelines/regulations of the Public Health Service Policy on Humane Care and Use of Laboratory Animals and the Animal Welfare Act, and under the approval of the University of Pittsburgh Institutional Animal Care and Use Committee.

Antibodies and reagents

Unless otherwise specified, all reagents were purchased from MilliporeSigma (St. Louis, MO). CK869, SMIFH2, ML141, and GSK269962

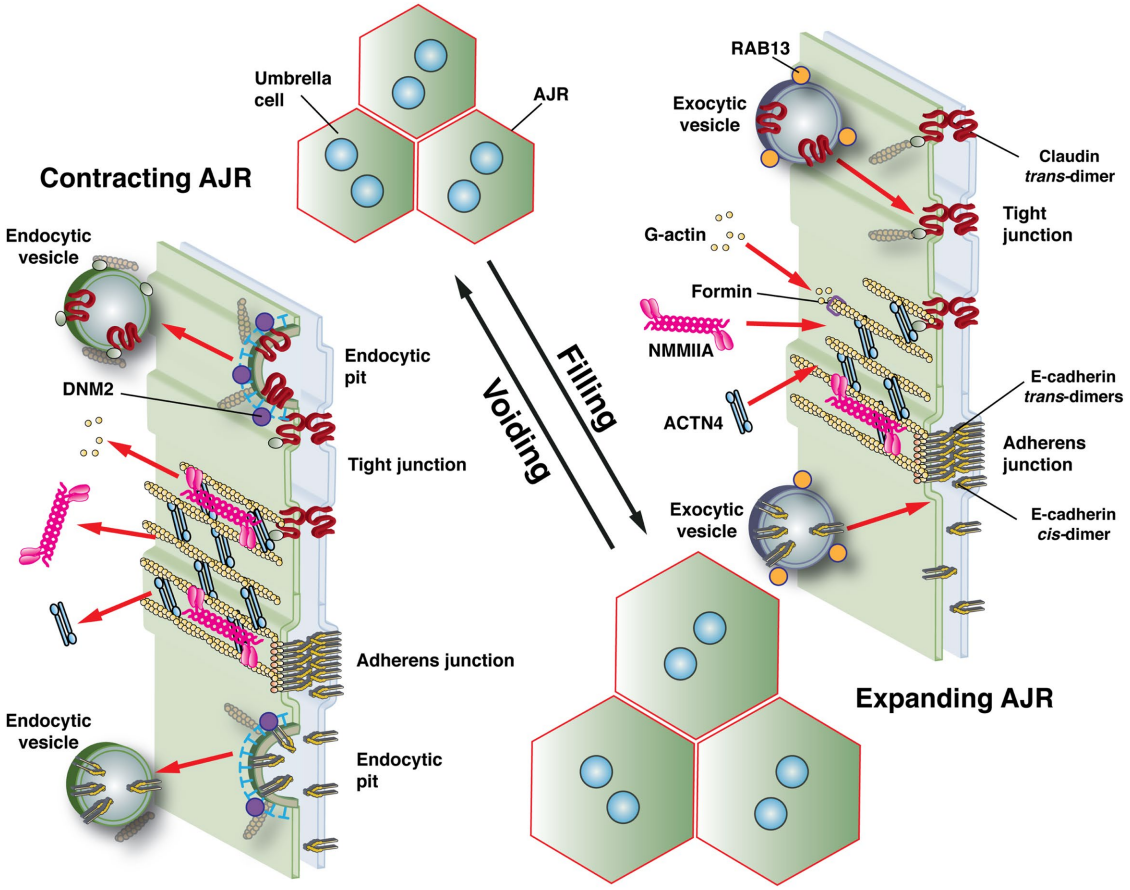

FIGURE 8: Model for AJR dynamics during bladder filling and voiding. During bladder filling the AJR expands in a process that requires formin-dependent actin polymerization. AJR expansion also requires RAB13-dependent exocytosis, likely of tight junction– and adherens junction–associated proteins. Although shown traveling in distinct vesicles, the tight-junction and adherens-junction proteins may travel in the same exocytic vesicles. Upon voiding, the AJR contracts in a process that requires NMMIIA-dependent constriction of the AJR-associated actomyosin cytoskeleton. Contraction also depends on DNM2-dependent endocytosis of AJR-associated proteins. It is unknown whether endocytosis is clathrin-dependent or -independent, or whether endocytic vesicles contain both tight junction– and adherens junction–associated proteins.

were purchased from Tocris Bioscience, Biotechne Corporation (Minneapolis, MN). Chemicals stocks were prepared in DMSO as 1000-fold stocks and stored at -20°C: cytochalasin D, 25 mg/ml; blebbistatin, 10 mM; brefeldin A, 5 mg/ml; cycloheximide, 100 mg/ml; Pitstop2, 30 mM; CK869, 100 mM; SMIFH2, 50 mM; ML141, 25 mM; GSK269962, 100 μM. They were diluted 1000-fold immediately before use. Primary antibodies used in this study were rabbit polyclonal claudin-8 (cat# 400700; Thermofisher Scientific, Waltham, MA), mouse monoclonal E-cadherin (cat# 610181; BD Transduction Laboratories, San Jose, CA), rabbit polyclonal nonmuscle myosin IIA (cat# 909801; Biolegend, San Diego, CA), rabbit polyclonal nonmuscle myosin IIB (cat# 909901; Biolegend), rabbit polyclonal nonmuscle myosin IIC (cat# PA5-66483; Thermofisher Scientific), rabbit polyclonal α-actinin-4 (cat# ALX-210-356; Enzo Life Sciences, New York, NY), rabbit polyclonal zonula occludens-1 (cat# 61-7300; Thermofisher Scientific), goat polyclonal platelet-derived growth factor-α (cat# AF1062; R&D Systems, Minneapolis, MN), rabbit polyclonal RAB13 (cat# NBP1-85799; Novus Biologicals, Centennial, CO) was used for Western blot, rabbit polyclonal RAB13 (cat# 07-794; Millipore Sigma) was used for immunofluorescence, mouse monoclonal RAB8A (cat# 610844; BD Transduction Laboratories), rabbit polyclonal RAB11A (cat# 71-5300; Thermofisher Scientific) and rabbit polyclonal HA (cat# SAB4300603; Millipore Sigma). Minimal cross-reacting Alexa488-, Cy5-, or horseradish peroxidase (HRP)-conjugated goat anti-mouse and goat-anti-rabbit and Alexa488-conjugated goat-anti-mouse secondary antibodies were purchased from Jackson ImmunoResearch (West Grove, PA). Rhodamine-phalloidin, Alexa594-phalloidin, and To-Pro-3 were purchased from Thermofisher Scientific.

Preparation of filled, voided, and quiescent bladders

Rats were sedated by inhalation of 3% (vol/vol) isofluorane and then injected subcutaneously with 1.35 g/kg urethane prepared fresh in dH_2O and sterile filtered through a 0.22 μm STERIFLIP-GP filter (Millipore Sigma) before use. Animals were allowed to reach proper anesthetic depth over a period of 2.5 h, which was confirmed by lack of a response to a toe pinch. Anesthetized rats allowed to undergo spontaneous filling were separated into three groups: filled, voided, and quiescent. All three groups were catheterized by inserting a 22-gauge Jelco IV catheter (trimmed to ~1 cm in length; Smiths-Medical, Minneapolis, MN) into the urethra. A three-way port was attached to the Luer fitting and, if necessary, the animals were subjected to Credé's maneuver to void their bladders before the start of the experiment. Subsequently, animals in the filled and voided groups had their catheter ports closed, and their bladders were allowed to fill over 2.5 h to an approximate final volume of 500 μl. After the 2.5-h filling period, animals in the voided group had their catheter ports reopened and were allowed to void for 5 min. The animals with quiescent bladders remained catheterized for the full 2.5-h time period, so the bladders remained in a relaxed state.

For drug filling/voiding assays, animals were anesthetized (Supplemental Figure S6A), as described above. A small incision was made in the lower portion of the abdomen, revealing the peritoneal cavity. The ureters were identified, cut, and sutured closed using 6-0, 13-mm Unify silk surgical sutures (AD Surgical, Sunnyvale, CA). The peritoneal incision was closed using the BD Autoclip wound closing system (Becton, Dickinson and Company, Parsippany, NJ). Subsequently, the animals were transurethrally catheterized and the Jelco IV catheter was secured using a surgical suture inserted below and then around the catheter. Animals were subjected to Credé's maneuver to void their bladders before the start of the experiment. Again, anesthetized rats were separated into three groups: filled, voided, and quiescent. The catheters were attached via their Luer fittings to 5-ml syringes mounted on a multisyringe pump (NE-1600; World Precision Instruments, Sarasota, FL). Syringes were loaded either with Kreb's buffer (110 mM NaCl, 25 mM $NaHCO_3$, 5.8 mM KCl, 1.2 mM $MgSO_4$, 4.8 mM KH_2PO_4, 11 mM glucose, 2 mM $CaCl_2$, gassed with 5% vol/vol CO_2) containing 0.1% (vol/vol) DMSO for controls, or with Kreb's buffer + drug for experimental groups. For groups *with* preincubation, 50 μl was pumped into the bladders over 5 min at a rate of 10 μl/min and incubated for 1 h (Supplemental Figure S6B). After the 1-h preincubation, the filled and voided groups had an additional 450 μl of Kreb's buffer ± drug pumped into the bladder over 45 min at a rate of 10 μl/min to a final volume of 500 μl. After the 45-min filling period, animals in the voided group had their catheter ports reopened and were allowed to void for 5 min (Supplemental Figure S6C). After the 1-h preincubation, the quiescent group had the syringe that was attached to the catheter port removed from the pump during the 45-min filling period, so that no additional liquid was instilled into the bladder and the animals ended the experiment with a total volume of 50 μl in the bladder lumen (Supplemental Figure S6D). For filled and voided groups without preincubation, 500 μl of Kreb's + DMSO or Kreb's + drug was pumped into the bladder over 30 min at a rate of 16.67 μl/min. After the 30-min filling period, animals in the voided group had their catheter ports reopened and were allowed to void for 5 min (Supplemental Figure S6E). The quiescent group had the syringe that was attached to the catheter port removed from the pump during the 30-min filling period, so that no liquid was instilled into the bladder (Supplemental Figure S6F).

At the end of the experiment, animals were perfusion-fixed. A thoracotomy was performed, the caudal vena cava was cut, and 50 ml of 100 mM sodium phosphate buffer (pH 7.4) at 37°C, was perfused through the left ventricle using an 18-gauge needle. Subsequently, the perfusate was switched to 100 mM sodium phosphate buffer (pH 7.4) containing 4% (wt/vol) paraformaldehyde. The bladders were excised, placed in Kreb's buffer containing 2% paraformaldehyde (wt/vol), cut open down their midline, and pinned out on a rubber mat, with minimal stretching, to expose the apicalmost umbrella cell layer. The tissues were stored at 4°C in 2% (wt/vol) paraformaldehyde until ready for processing for whole-mount microscopy. Alternatively, the fixed bladder was cut into quarters, cryoprotected by incubating in 35% (wt/vol) sucrose in phosphate-buffered saline (PBS) until the tissue sank, embedded in optimal cutting temperature (OCT) compound (Scigen, Gardena, CA), and frozen in 10 mm × 10 mm × 5 mm Tissue-Tek cryomolds (Sakura Finetek, Torrance, CA) on dry ice. Frozen tissue blocks were stored at -80°C in water-tight plastic bags before sectioning.

Indirect immunofluorescence labeling and image capture

Frozen tissue blocks were sectioned at 5 μm thick using a CM1950 cryostat (Leica Biosystems, Wetzlar, Germany) and collected on Fisherbrand Superfrost Plus microscope slides (Thermo Fisher Scientific). Immunofluorescence labeling of whole-mount and cryosectioned bladder tissue was performed at room temperature, unless otherwise indicated. Tissue was washed three times with PBS for 5 min. Unreacted paraformaldehyde was quenched and the tissue was permeabilized by washing tissue for 10 min with PBS containing 0.1% (vol/vol) Triton X-100, 20 mM glycine (pH 8.0), and 75 mM ammonium chloride. Tissue was washed three times with PBS for 5 min and then three times quickly with block solution (which contained

0.7% [wt/vol] fish-skin gelatin, 0.025% [wt/vol] saponin, and 0.02% [wt/vol] sodium azide, all dissolved in PBS). Tissue was next incubated for 30 min in block solution and then incubated overnight at 4°C in block solution containing the primary antibody. After incubation with the primary antibody, the tissue was rinsed three times quickly with block solution and then three times for 5 min with block solution. Subsequently, the tissue was incubated for 1 h with secondary antibody diluted in block solution. Tissue was then rinsed three times quickly with block solution, three times for 5 min with block solution, and then three times quickly with PBS. The antibodies were postfixed with 4% (wt/vol) paraformaldehyde in 100 mM sodium phosphate buffer (pH 7.4) for 10 min (tissue sections) or 20 min (whole-mount), after which the tissue was rinsed three times quickly with PBS. Finally, the paraformaldehyde was quenched, as described above, and rinsed three times quickly with PBS. After being labeled, tissue sections were covered with a drop of Slowfade Diamond antifade mountant (Thermo Fisher Scientific), covered with a Gold Seal cover glass (number 1.5, Thermo Fisher Scientific), and sealed around the edges with a thin layer of nail polish (Electron Microscopy Sciences, Hatfield, PA). Whole-mount tissue was placed, apical surface facing up, within a square well created with nail polish to which a drop of Slowfade Diamond antifade mountant was added. An additional drop of mountant was added to the top of the tissue. A cover glass was placed over the tissue and sealed around its edges with a thin layer of nail polish.

Confocal images were captured using a Leica HCX PL APO 40 × 1.25 NA oil objective, a Leica HCX PL APO 63 × 1.3 NA glycerol objective, or a Leica 100 × 1.4 NA oil objective on a Leica TCS SP5 CW-STED confocal microscope (in normal confocal mode). The HyD detectors were set at their maximal values, laser output was used to control image "brightness," and eight-bit images were collected using eight-line averages in combination with six-frame averages. For tissue sections, serial 0.2- µm *Z*-sections were acquired. For whole-mounted tissues, serial 0.5-µm *Z*-sections were acquired. Maximum intensity projections of each sample were generated using Volocity 4-D software (Perkin Elmers, Waltham, MA) and exported as TIFF files. Alternatively, single wide-field images were captured using a Leica HCX PL APO 40 × 1.25 NA oil objective on a Leica DM6000 B wide-field fluorescence microscope. Images were captured using a Retiga 4000R digital camera (Q Imaging, Surrey, CA). Images were contrast-corrected in Adobe Photoshop CC2017 (Adobe, Mountain View, CA), and composite images were created using Adobe Illustrator CC2017.

Quantitation of AJR perimeter

Whole-mount tissue from filled, voided, and quiescent bladders was processed and imaged as described above. Twenty random images, five images per bladder quadrant, were collected. Each image was opened in FIJI and the "set scale" command was selected from the "analyze" drop-down menu. The distance in pixels per known distance was entered and the "global" check box was selected. The "set measurements" command was selected from the "analyze" drop-down menu and the "perimeter" option was selected. For images that contained five or fewer umbrella cells (e.g., those from filled bladders), the perimeter of the AJR (perimeter$_{AJR}$) of each cell was measured by following the contours of the AJR using the "polygon" tool and selecting "measure" from the "analyze" drop-down menu. Perimeter$_{AJR}$ values for each image were averaged. For images than contained more than five umbrella cells (e.g., those from voided bladders), we employed a random number generator to choose five representative cells to measure. In this case, each of the cells in the image was numbered using the "text tool." The "Sequence Generator" option on www.Random.org was chosen and the number of cells in the image was input. Using the first five numbers of the random sequence generated, the perimeters of the corresponding cells were measured using the technique described above. Again, an average of all five measurements was made. The average umbrella cell perimeter$_{AJR}$ for an individual bladder was calculated by determining the mean of the perimeter$_{AJR}$ for each of the 20 random images.

Nonlinear regression analysis of filling data

Bladders were filled with a syringe pump (as described above) with 0, 500, 1000, or 1500 µl ($n = 3$ for each group) over 45 min. Average Perimeter$_{AJR}$ per umbrella cell was estimated for each bladder, as described above, and these values were fitted to a single exponential using Prism's (Graphpad, San Diego, CA) nonlinear regression curve fit analysis.

Preparation of chemically competent AdEasier-1 cells

AdeEsier-1 cells (Addgene, Watertown, MA; bacterial strain #16399) were grown overnight in 5 ml Luria–Bertani (LB) broth with 1:1000 streptomycin (30 µg/ml) and 1:1000 ampicillin (100 µg/ml) on a shaker at 37°C. Subsequently, the 5-ml culture was diluted into 100 ml LB broth with streptomycin and ampicillin and shaken at 37°C for 1.5 h, or until the culture reached an OD_{600} of 0.5. The culture was spun for 10 min at 2057 RCF at 4°C in a 5810R centrifuge outfitted with an F-34-6-38 fixed-angle rotor (Eppenderf, Hamburg, DE), and the pellet was resuspended in 20 ml, ice-cold 100 mM $MgCl_2$ and incubated on ice for 20 min. The resuspension was centrifuged for an additional 10 min at relative centrifugal force (RCF) 2057 at 4°C and the pellet was resuspended in 2 ml sterile, ice-cold $CaCl_2$ in 15% vol/vol glycerol. Cells were aliquoted into tubes prechilled to -80°C and stored until use at –80°C.

Production of adenoviruses and summary of viral constructs

DN-RAB13-GFP adenovirus was produced using the AdEasy system. A gBlock (Integrated DNA Technologies, Coralville, IA) encoding GFP-tagged rat *Rab13* flanked by *Xho*I and *Hin*dIII restriction sites was cloned into pShuttleCMV (Addgene; plasmid #16403). DN-RAB13-GFP (T22N) was generated by mutating pShuttleCMV-*Rab13*-GFP using Qiagen QuikChange II Site-Directed Mutagenesis kit (Agilent Technologies, Santa Clara, CA) using the primer 5′-TCG GGG GTG GGC AAG AAT TGT CTC ATC ATT CGC TT-3′. The construct was confirmed by sequencing. DN-*Rab13*-GFP was linearized with *Pme*I and recombined with the adenoviral backbone in chemically competent AdEasier-1 cells, described above. Recombined pShuttleCMV-DN-*Rab13*-GFP cDNA was extracted from AdEasier-1 cells using a QIAprep Spin miniprep kit (Qiagen, Hilden, DE). This cDNA was transformed into *recA*-deficient XL10-Gold ultracompetent cells (Agilent Technologies). Recombined cDNA was extracted with a NucleoBond Xtra endotoxin-free midiprep kit (Macherey-Nagel, Bethlehem, PA) and linearized with *Pac*I. Adenovirus encoding DN-Rab13-GFP was produced by transfection of AD293 cells with the linearized cDNA (Agilent Technologies). After ~3 wk, cells were harvested and the virus was extracted by repeated freeze/thaw cycles in liquid nitrogen and in a 37°C water bath, respectively. The crude adenovirus was subsequently purified by loading it onto a CsCl step gradient made of low-density CsCl (323 g/l) layered on top of high-density CsCl (530 g/l) prepared in sterile 100 mM Tris/10 mM EDTA (pH 7.4) and by spinning for 1 h at RCF 151,263 at 4°C in an Optima L-80 XP ultracentrifuge outfitted with an SW41 Ti rotor (Beckman Coulter Life Sciences, Indianapolis, IN). The viral band found at the interface of the low-density and high-density

CsCl layers was extracted using a 12-gauge needle and loaded onto a Sephadex G-25 PD10 desalting column (GE Healthcare Life Sciences, Pittsburgh, PA) preequilibrated with sterile 10% glycerol in PBS. Five hundred microliter fractions were collected. The virus was found in fractions 9, 10, and 11 at concentrations ranging from 25 to 35 million IVP/μl.

DN-RAB8A-GFP (T22N) and RAB11A-GFP (S25N) adenoviruses were described previously (Khandelwal *et al.*, 2013). Crude adenovirus encoding DN-DNM1-HA (K44A) was a kind gift from Sandra Schmid (UT Southwestern, Dallas, TX) and was amplified and purified in house. DN-RHOA-GFP (V19N) adenovirus was described previously (Khandelwal *et al.*, 2010).

In situ adenoviral transduction

In situ transduction was performed as described previously (Khandelwal *et al.*, 2008). Briefly, rats were sedated with 3% (vol/vol) isofluorane and a 22-gauge Jelco IV catheter (Smith Medicals), trimmed to ~1 cm in length, was inserted into the bladder via the urethra. The bladder was rinsed with PBS and filled with 400 μl of 0.1% wt/vol dodecyl-β-D-maltoside dissolved in PBS. The urethra was clamped and after 5 min was unclamped to allow the detergent to void. The latter step was facilitated by performing Credé's maneuver. Subsequently, the bladder was filled with 400 μl PBS containing adenoviruses expressing the constructs described above (2.0×10^8 infectious virus particles, typically in a volume of 2–10 μl for each virus). The urethra was clamped, and after 30 min it was unclamped and the virus solution was allowed to void. The bladder was rinsed with PBS, anesthesia was discontinued, and the rats were allowed to revive. The rats were killed 3 d posttransduction to allow time for the umbrella cells to regain their normal morphology.

Lysate preparation and Western blotting

To obtain rat epithelial bladder lysates, rat bladders were excised, cut down the midline, and pinned open on a rubber mat to expose the apical umbrella cell layer. A 0.5% (wt/vol) SDS-lysis buffer (100 mM NaCl, 50 mM tetraethylammonium, 5 mM EDTA, 0.2% wt/vol NaN3, and 0.5% wt/vol SDS; 50 μl) containing 0.5 mM phenylmethylsulfonylfluoride (PMSF) and 1:100 dilution of a protease inhibitor cocktail (PIC; MilliporeSigma) was pipetted onto the apical surface of the tissue. Epithelial cells were gently scraped with a rubber cell scraper (Sarstedt, Nümbrecht, Germany) and deposited in a 1.5-ml microcentrifuge tube. This process was repeated once for a final volume of 100 μl of lysate. For HeLa cell lysates, cells were grown to confluence on six-well tissue culture dishes (Corning, Corning, NY). The 0.5% SDS-lysis buffer containing 0.5 mM PMSF and a 1:100 dilution of PIC (MilliporeSigma; 500 μl) was pipetted onto the apical surface of the cells. The cells were gently scraped with a rubber cell scraper (Sarstedt) and deposited in a 1.5-ml microcentrifuge tube. All lysates were shaken at 4°C at 3000 RPM for 15 min in a MixMate benchtop mixer (Eppendorf, Hamburg, Germany). Rat bladder lysates (50 μg) and HeLa cell lysates (10 μg) were diluted 1:1 with 2× Laemmli sample buffer (Bio-Rad, Hercules, CA) supplemented with 0.05% vol/vol β–mercapto-ethanol and incubated at 95°C for 5 min. The proteins were resolved on 12% Criterion TGX SDS-polyacrylamide gels (Bio-Rad) and transferred for 30 min in 100 mM CAPS buffer (pH 11) at 400 mA onto Immobilon-P membranes (MilliporeSigma). The membrane was blocked with 5% wt/vol bovine serum albumin (BSA) in Tris-buffered saline + Tween (TBST, 2.68 mM KCl, 0.5 M NaCl, 25 mM Tris–HCl, pH 8.0, and 0.05% vol/vol Tween 20) for 45 min at room temperature, washed three times for 10 min with TBST, and incubated overnight at 4°C with 1:1000 anti-RAB8A, RAB11A, or RAB13 antibody diluted in TBST containing 1% wt/vol BSA. After the overnight incubation, the membrane was washed three times for 10 min with TBST, incubated for 1 h with rotation at room temperature with the appropriate HRP-conjugated goat anti-mouse or goat anti-rabbit secondary antibody diluted 1:5000 in TBST containing 1% wt/vol BSA, and then washed three times for 10 min with TBST. Immunoreactive protein species were visualized using Pierce SuperSignal West Pico PLUS Chemiluminescent Substrate (Thermo Fisher Scientific) and image capture was performed using a Chemidoc Touch imaging system (Bio-Rad).

Data and statistical analysis

Data are reported as mean ± SEM. Statistically significant differences were determined using one-way analysis of variance (ANOVA) with Dunnett's correction. A p value ≤ 0.05 was considered statistically significant. Alternatively, we used a paired two-tailed t test with a p value ≤ 0.05 considered statistically significant.

ACKNOWLEDGMENTS

This work was supported by grants from the National Institute of Diabetes and Digestive and Kidney Diseases of the National Institutes of Health: F31-DK117547-02 (to A.F.E.); R01-DK104287 and P30-DK079307 (to G.A.); and R56-DC013048 (to M.E.R.); and by the Kidney Imaging Core of the Pittsburgh Center for Kidney Research (P30-DK079307).

REFERENCES

Acharya P, Beckel J, Ruiz WG, Wang E, Rojas R, Birder L, Apodaca G (2004). Distribution of the tight junction proteins ZO-1, occludin, and claudin-4, -8, and -12 in bladder epithelium. Am J Physiol Renal Physiol 287, F305–F318.

Akao S, Oya M, Akiyama H, Ishikawa H (2000). The tight junction of pancreatic exocrine cells is a morphometrically dynamic structure altered by intraductal hypertension. J Gastroenterol 35, 758–767.

Allingham JS, Smith R, Rayment I (2005). The structural basis of blebbistatin inhibition and specificity for myosin II. Nat Struct Mol Biol 12, 378–379.

Amano M, Ito M, Kimura K, Fukata Y, Chihara K, Nakano T, Matsuura Y, Kaibuchi K (1996). Phosphorylation and activation of myosin by Rho-associated kinase (Rho-kinase). J Biol Chem 271, 20246–20249.

Apodaca G (2001a). Endocytic traffic in polarized epithelial cells: role of the actin and microtubule cytoskeleton. Traffic 2, 149–159.

Apodaca G (2001b). Stretch-regulated exocytosis of discoidal vesicles in urinary bladder epithelium. Urology 57, 103–104.

Apodaca G (2002). Modulation of membrane traffic by mechanical stimuli. Am J Physiol Renal Physiol 282, F179–F190.

Arnold TR, Stephenson RE, Miller AL (2017). Rho GTPases and actomyosin: Partners in regulating epithelial cell–cell junction structure and function. Exp Cell Res 358, 20–30.

Balda MS, Matter K (2008). Tight junctions at a glance. J Cell Sci 121, 3677–3682.

Balda MS, Matter K (2016). Tight junctions as regulators of tissue remodelling. Curr Opin Cell Biol 42, 94–101.

Bardet PL, Guirao B, Paoletti C, Serman F, Leopold V, Bosveld F, Goya Y, Mirouse V, Graner F, Bellaiche Y (2013). PTEN controls junction lengthening and stability during cell rearrangement in epithelial tissue. Dev Cell 25, 534–546.

Borges RM, Lamers ML, Forti FL, Santos MF, Yan CY (2011). Rho signaling pathway and apical constriction in the early lens placode. Genesis 49, 368–379.

Butler LC, Blanchard GB, Kabla AJ, Lawrence NJ, Welchman DP, Mahadevan L, Adams RJ, Sanson B (2009). Cell shape changes indicate a role for extrinsic tensile forces in *Drosophila* germ-band extension. Nat Cell Biol 11, 859–864.

Carattino MD, Prakasam HS, Ruiz WG, Clayton DR, McGuire M, Gallo LI, Apodaca G (2013). Bladder filling and voiding affect umbrella cell tight junction organization and function. Am J Physiol Renal Physiol 305, F1158–F1168.

Cavanaugh KJ Jr, Oswari J, Margulies SS (2001). Role of stretch on tight junction structure in alveolar epithelial cells. Am J Respir Cell Mol Biol 25, 584–591.

Charras G, Yap AS (2018). Tensile forces and mechanotransduction at cell–cell junctions. Curr Biol 28, R445–R457.
Chen Y, Guo X, Deng FM, Liang FX, Sun W, Ren M, Izumi T, Sabatini DD, Sun TT, Kreibich G (2003). Rab27b is associated with fusiform vesicles and may be involved in targeting uroplakins to urothelial apical membranes. Proc Natl Acad Sci USA 100, 14012–14017.
Chung YC, Wei WC, Huang SH, Shih CM, Hsu CP, Chang KJ, Chao WT (2014). Rab11 regulates E-cadherin expression and induces cell transformation in colorectal carcinoma. BMC Cancer 14, 587.
Cohen TS, Gray Lawrence G, Khasgiwala A, Margulies SS (2010). MAPK activation modulates permeability of isolated rat alveolar epithelial cell monolayers following cyclic stretch. PLoS One 5, e10385.
Costa M, Raich W, Agbunag C, Leung B, Hardin J, Priess JR (1998). A putative catenin–cadherin system mediates morphogenesis of the Caenorhabditis elegans embryo. J Cell Biol 141, 297–308.
Croise P, Estay-Ahumada C, Gasman S, Ory S (2014). Rho GTPases, phosphoinositides, and actin: a tripartite framework for efficient vesicular trafficking. Small GTPases 5, e29469.
Desclozeaux M, Venturato J, Wylie FG, Kay JG, Joseph SR, Le HT, Stow JL (2008). Active Rab11 and functional recycling endosome are required for E-cadherin trafficking and lumen formation during epithelial morphogenesis. Am J Physiol Cell Physiol 295, C545–C556.
Doe C, Bentley R, Behm DJ, Lafferty R, Stavenger R, Jung D, Bamford M, Panchal T, Grygielko E, Wright LL, *et al.* (2007). Novel Rho kinase inhibitors with anti-inflammatory and vasodilatory activities. J Pharmacol Exp Ther 320, 89–98.
Doherty GJ, McMahon HT (2009). Mechanisms of endocytosis. Annu Rev Biochem 78, 857–902.
Duan Y, Gotoh N, Yan Q, Du Z, Weinstein AM, Wang T, Weinbaum S (2008). Shear-induced reorganization of renal proximal tubule cell actin cytoskeleton and apical junctional complexes. Proc Natl Acad Sci USA 105, 11418–11423.
Dutta D, Williamson CD, Cole NB, Donaldson JG (2012). Pitstop 2 is a potent inhibitor of clathrin-independent endocytosis. PLoS One 7, e45799.
Ebrahim S, Fujita T, Millis BA, Kozin E, Ma X, Kawamoto S, Baird MA, Davidson M, Yonemura S, Hisa Y, *et al.* (2013). NMII forms a contractile transcellular sarcomeric network to regulate apical cell junctions and tissue geometry. Curr Biol 23, 731–736.
Efimova N, Svitkina TM (2018). Branched actin networks push against each other at adherens junctions to maintain cell–cell adhesion. J Cell Biol 217, 1827–1845.
Fanning AS, Van Itallie CM, Anderson JM (2012). Zonula occludens-1 and -2 regulate apical cell structure and the zonula adherens cytoskeleton in polarized epithelia. Mol Biol Cell 23, 577–590.
Farquhar MG, Palade GE (1963). Junctional complexes in various epithelia. J Cell Biol 17, 375–412.
Gallo LI, Dalghi MG, Clayton DR, Ruiz WG, Khandelwal P, Apodaca G (2018). RAB27B requirement for stretch-induced exocytosis in bladder umbrella cells. Am J Physiol Cell Physiol 314, C349-C365.
Greven H, Robenek H (1980). Intercellular junctions in the uterine epithelium of *Salamandra salamandra* (L.) (Amphibia, Urodela). A freeze-fracture study. Cell Tissue Res 212, 163–172.
Homem CC, Peifer M (2008). Diaphanous regulates myosin and adherens junctions to control cell contractility and protrusive behavior during morphogenesis. Development 135, 1005–1018.
Itoh K, Ossipova O, Sokol SY (2014). GEF-H1 functions in apical constriction and cell intercalations and is essential for vertebrate neural tube closure. J Cell Sci 127, 2542–2553.
Jegou A, Carlier MF, Romet-Lemonne G (2013). Formin mDia1 senses and generates mechanical forces on actin filaments. Nat Commun 4, 1883.
Jewett CE, Vanderleest TE, Miao H, Xie Y, Madhu R, Loerke D, Blankenship JT (2017). Planar polarized Rab35 functions as an oscillatory ratchet during cell intercalation in the *Drosophila* epithelium. Nat Commun 8, 476.
Kaksonen M, Roux A (2018). Mechanisms of clathrin-mediated endocytosis. Nat Rev Mol Cell Biol 19, 313–326.
Khandelwal P, Abraham SN, Apodaca G (2009). Cell biology and physiology of the uroepithelium. Am J Physiol Renal Physiol 297, F1477–F1501.
Khandelwal P, Prakasam HS, Clayton DR, Ruiz WG, Gallo LI, van Roekel D, Lukianov S, Peranen J, Goldenring JR, Apodaca G (2013). A Rab11a-Rab8a-Myo5B network promotes stretch-regulated exocytosis in bladder umbrella cells. Mol Biol Cell 24, 1007–1019.
Khandelwal P, Ruiz WG, Apodaca G (2010). Compensatory endocytosis in bladder umbrella cells occurs through an integrin-regulated and RhoA- and dynamin-dependent pathway. EMBO J 29, 1961–1975.
Khandelwal P, Ruiz G, Balestreire-Hawryluk E, Weisz OA, Goldenring JA, Apodaca G (2008). Rab11a-dependent exocytosis of discoidal/fusiform vesicles in bladder umbrella cells. Proc Natl Acad Sci USA 105, 15773–15778.
Kjos I, Vestre K, Guadagno NA, Borg Distefano M, Progida C (2018). Rab and Arf proteins at the crossroad between membrane transport and cytoskeleton dynamics. Biochim Biophys Acta Mol Cell Res 1865, 1397–1409.
Klausner RD, Donaldson JG, Lippincott-Schwartz J (1992). Brefeldin A: insights into the control of membrane traffic and organelle structure. J Cell Biol 116, 1071–1080.
Koga A, Todo S (1978). Morphological and functional changes in the tight junctions of the bile canaliculi induced by bile duct ligation. Cell Tissue Res 195, 267–276.
Koh BH, Roy R, Hollywood MA, Thornbury KD, McHale NG, Sergeant GP, Hatton WJ, Ward SM, Sanders KM, Koh SD (2012). Platelet-derived growth factor receptor-alpha cells in mouse urinary bladder: a new class of interstitial cells. J Cell Mol Med 16, 691–700.
Kohler K, Louvard D, Zahraoui A (2004). Rab13 regulates PKA signaling during tight junction assembly. J Cell Biol 165, 175–180.
Kolesnikov T, Beckendorf SK (2007). 18 wheeler regulates apical constriction of salivary gland cells via the Rho-GTPase-signaling pathway. Dev Biol 307, 53–61.
Kong D, Wolf F, Grosshans J (2017). Forces directing germ-band extension in *Drosophila* embryos. Mech Dev 144, 11–22.
Lamaze C, Dujeancourt A, Baba T, Lo CG, Benmerah A, Dautry-Varsat A (2001). Interleukin 2 receptors and detergent-resistant membrane domains define a clathrin-independent endocytic pathway. Mol Cell 7, 661–671.
Lee JY, Harland RM (2010). Endocytosis is required for efficient apical constriction during *Xenopus* gastrulation. Curr Biol 20, 253–258.
Levayer R, Pelissier-Monier A, Lecuit T (2011). Spatial regulation of Dia and Myosin-II by RhoGEF2 controls initiation of E-cadherin endocytosis during epithelial morphogenesis. Nat Cell Biol 13, 529–540.
Lewis SA, de Moura JL (1982). Incorporation of cytoplasmic vesicles into apical membrane of mammalian urinary bladder epithelium. Nature 297, 685–688.
Liu Z, Tan JL, Cohen DM, Yang MT, Sniadecki NJ, Ruiz SA, Nelson CM, Chen CS (2010). Mechanical tugging force regulates the size of cell–cell junctions. Proc Natl Acad Sci USA 107, 9944–9949.
Lock JG, Stow JL (2005). Rab11 in recycling endosomes regulates the sorting and basolateral transport of E-cadherin. Mol Biol Cell 16, 1744–1755.
Ma L, Rohatgi R, Kirschner MW (1998). The Arp2/3 complex mediates actin polymerization induced by the small GTP-binding protein Cdc42. Proc Natl Acad Sci USA 95, 15362–15367.
Marzesco AM, Dunia I, Pandjaitan R, Recouvreur M, Dauzonne D, Benedetti EL, Louvard D, Zahraoui A (2002). The small GTPase Rab13 regulates assembly of functional tight junctions in epithelial cells. Mol Biol Cell 13, 1819–1831.
Marzesco AM, Zahraoui A (2005). Assay of Rab13 in regulating epithelial tight junction assembly. Methods Enzymol 403, 182–193.
Mateus AM, Gorfinkiel N, Schamberg S, Martinez Arias A (2011). Endocytic and recycling endosomes modulate cell shape changes and tissue behaviour during morphogenesis in *Drosophila*. PLoS One 6, e18729.
Mayor S, Parton RG, Donaldson JG (2014). Clathrin-independent pathways of endocytosis. Cold Spring Harb Perspect Biol 6, a016758.
Metz J, Aoki A, Merlo M, Forssmann WG (1977). Morphological alterations and functional changes of interhepatocellular junctions induced by bile duct ligation. Cell Tissue Res 182, 299–310.
Metz J, Merlo M, Billich H, Forssmann WG (1978). Exocrine pancreas under experimental conditions. IV. Alterations of intercellular junctions between acinar cells following pancreatic duct ligation. Cell Tissue Res 186, 227–240.
Nolen BJ, Tomasevic N, Russell A, Pierce DW, Jia Z, McCormick CD, Hartman J, Sakowicz R, Pollard TD (2009). Characterization of two classes of small molecule inhibitors of Arp2/3 complex. Nature 460, 1031–1034.
Park M, Kim HJ, Lim B, Wylegala A, Toborek M (2013). Methamphetamine-induced occludin endocytosis is mediated by the Arp2/3 complex-regulated actin rearrangement. J Biol Chem 288, 33324–33334.
Pinheiro D, Bellaiche Y (2018). Mechanical force-driven adherens junction remodeling and epithelial dynamics. Dev Cell 47, 3–19.
Pitelka DR, Hamamoto ST, Duafala JG, Nemanic MK (1973). Cell contacts in the mouse mammary gland. I. Normal gland in postnatal development and the secretory cycle. J Cell Biol 56, 797–818.

Pitelka DR, Taggart BN (1983). Mechanical tension induces lateral movement of intramembrane components of the tight junction: studies on mouse mammary cells in culture. J Cell Biol 96, 606–612.
Ramesh N, Memarzadeh B, Ge Y, Frey D, VanRoey M, Rojas V, Yu DC (2004). Identification of pretreatment agents to enhance adenovirus infection of bladder epithelium. Mol Ther 10, 697–705.
Rizvi SA, Neidt EM, Cui J, Feiger Z, Skau CT, Gardel ML, Kozmin SA, Kovar DR (2009). Identification and characterization of a small molecule inhibitor of formin-mediated actin assembly. Chem Biol 16, 1158–1168.
Rubsam M, Broussard JA, Wickstrom SA, Nekrasova O, Green KJ, Niessen CM (2018). Adherens junctions and desmosomes coordinate mechanics and signaling to orchestrate tissue morphogenesis and function: an evolutionary perspective. Cold Spring Harb Perspect Biol 10, a029207.
Sai X, Yonemura S, Ladher RK (2014). Junctionally restricted RhoA activity is necessary for apical constriction during phase 2 inner ear placode invagination. Dev Biol 394, 206–216.
Samak G, Gangwar R, Crosby LM, Desai LP, Wilhelm K, Waters CM, Rao R (2014). Cyclic stretch disrupts apical junctional complexes in Caco-2 cell monolayers by a JNK-2-, c-Src-, and MLCK-dependent mechanism. Am J Physiol Gastrointest Liver Physiol 306, G947–G958.
Schneider-Poetsch T, Ju J, Eyler DE, Dang Y, Bhat S, Merrick WC, Green R, Shen B, Liu JO (2010). Inhibition of eukaryotic translation elongation by cycloheximide and lactimidomycin. Nat Chem Biol 6, 209–217.
Schwayer C, Sikora M, Slovakova J, Kardos R, Heisenberg CP (2016). Actin rings of power. Dev Cell 37, 493–506.
Shaye DD, Casanova J, Llimargas M (2008). Modulation of intracellular trafficking regulates cell intercalation in the *Drosophila* trachea. Nat Cell Biol 10, 964–970.
Sluysmans S, Vasileva E, Spadaro D, Shah J, Rouaud F, Citi S (2017). The role of apical cell–cell junctions and associated cytoskeleton in mechanotransduction. Biol Cell 109, 139–161.
Song MJ, Davidovich N, Lawrence GG, Margulies SS (2016). Superoxide mediates tight junction complex dissociation in cyclically stretched lung slices. J Biomech 49, 1330–1335.
Soulet F, Schmid SL, Damke H (2006). Domain requirements for an endocytosis-independent, isoform-specific function of dynamin-2. Exp Cell Res 312, 3539–3545.
Spadaro D, Le S, Laroche T, Mean I, Jond L, Yan J, Citi S (2017). Tension-dependent stretching activates ZO-1 to control the junctional localization of its interactors. Curr Biol 27, 3783–3795 e3788.
Surviladze Z, Waller A, Strouse JJ, Bologa C, Ursu O, Salas V, Parkinson JF, Phillips GK, Romero E, Wandinger-Ness A, *et al*. (2010). A potent and selective inhibitor of Cdc42 GTPase. In: Probe Reports from the NIH Molecular Libraries Program, Bethesda (MD).
Takeichi M (2018). Multiple functions of alpha-catenin beyond cell adhesion regulation. Curr Opin Cell Biol 54, 24–29.
Thi MM, Tarbell JM, Weinbaum S, Spray DC (2004). The role of the glycocalyx in reorganization of the actin cytoskeleton under fluid shear stress: a "bumper-car" model. Proc Natl Acad Sci USA 101, 16483–16488.
Tornavaca O, Chia M, Dufton N, Almagro LO, Conway DE, Randi AM, Schwartz MA, Matter K, Balda MS (2015). ZO-1 controls endothelial adherens junctions, cell-cell tension, angiogenesis, and barrier formation. J Cell Biol 208, 821–838.
Truschel ST, Wang E, Ruiz WG, Leung SM, Rojas R, Lavelle J, Zeidel M, Stoffer D, Apodaca G (2002). Stretch-regulated exocytosis/endocytosis in bladder umbrella cells. Mol Biol Cell 13, 830–846.
Tzima E, Irani-Tehrani M, Kiosses WB, Dejana E, Schultz DA, Engelhardt B, Cao G, DeLisser H, Schwartz MA (2005). A mechanosensory complex that mediates the endothelial cell response to fluid shear stress. Nature 437, 426–431.
Valentijn K, Valentijn JA, Jamieson JD (1999). Role of actin in regulated exocytosis and compensatory membrane retrieval: insights from an old acquaintance. Biochem Biophys Res Commun 266, 652–661.
Vogler G, Liu J, Iafe TW, Migh E, Mihaly J, Bodmer R (2014). Cdc42 and formin activity control non-muscle myosin dynamics during *Drosophila* heart morphogenesis. J Cell Biol 206, 909–922.
von Kleist L, Stahlschmidt W, Bulut H, Gromova K, Puchkov D, Robertson MJ, MacGregor KA, Tomilin N, Pechstein A, Chau N, *et al*. (2011). Role of the clathrin terminal domain in regulating coated pit dynamics revealed by small molecule inhibition. Cell 146, 471–484.
Wang E, Pennington JG, Goldenring JR, Hunziker W, Dunn KW (2001). Brefeldin A rapidly disrupts plasma membrane polarity by blocking polar sorting in common endosomes of MDCK cells. J Cell Sci 114, 3309–3321.
Wankel B, Ouyang J, Guo X, Hadjiolova K, Miller J, Liao Y, Tham DK, Romih R, Andrade LR, Gumper I, *et al*. (2016). Sequential and compartmentalized action of Rabs, SNAREs, and MAL in the apical delivery of fusiform vesicles in urothelial umbrella cells. Mol Biol Cell 27, 1621–1634.
Watson CJ, Rowland M, Warhurst G (2001). Functional modeling of tight junctions in intestinal cell monolayers using polyethylene glycol oligomers. Am J Physiol Cell Physiol 281, C388–C397.
Welz T, Wellbourne-Wood J, Kerkhoff E (2014). Orchestration of cell surface proteins by Rab11. Trends Cell Biol 24, 407–415.
Woichansky I, Beretta CA, Berns N, Riechmann V (2016). Three mechanisms control E-cadherin localization to the zonula adherens. Nat Commun 7, 10834.
Yamamura R, Nishimura N, Nakatsuji H, Arase S, Sasaki T (2008). The interaction of JRAB/MICAL-L2 with Rab8 and Rab13 coordinates the assembly of tight junctions and adherens junctions. Mol Biol Cell 19, 971–983.
Yao M, Qiu W, Liu R, Efremov AK, Cong P, Seddiki R, Payre M, Lim CT, Ladoux B, Mege RM, Yan J (2014). Force-dependent conformational switch of alpha-catenin controls vinculin binding. Nat Commun 5, 4525.
Yu JC, Fernandez-Gonzalez R (2016). Local mechanical forces promote polarized junctional assembly and axis elongation in *Drosophila*. Elife 5.
Yu W, Khandelwal P, Apodaca G (2009). Distinct apical and basolateral membrane requirements for stretch-induced membrane traffic at the apical surface of bladder umbrella cells. Mol Biol Cell 20, 282–295.
Zhang HM, Ji HH, Ni T, Ma RN, Wang A, Li XD (2017). Characterization of blebbistatin inhibition of smooth muscle myosin and nonmuscle myosin-2. Biochemistry 56, 4235–4243.
Zhou K, Muroyama A, Underwood J, Leylek R, Ray S, Soderling SH, Lechler T (2013). Actin-related protein2/3 complex regulates tight junctions and terminal differentiation to promote epidermal barrier formation. Proc Natl Acad Sci USA 110, E3820–E3829.